

1 **Effect of Different Emission Inventories on Modeled Ozone**  
2 **and Carbon Monoxide in Southeast Asia**

3 **T. Amnuaylojaroen<sup>1,2</sup>, M. C. Barth<sup>2</sup>, L. K. Emmons<sup>2</sup>, G. R. Carmichael<sup>3</sup>, J.**  
4 **Kreasuwun<sup>1,4</sup>, S. Prasitwattanaseree<sup>5</sup> and S. Chantara<sup>1</sup>**

5 [1]{Environmental Science Program and the Center for Environmental Health, Toxicology  
6 and Management of Chemical, Chiang Mai University, Faculty of Science, Chiang Mai,  
7 Thailand}

8 [2]{Atmospheric Chemistry Division (ACD), National Center for Atmospheric Research  
9 (NCAR), Boulder, Colorado USA}

10 [3]{Center for Global and Regional Environmental Research, The University of Iowa, Iowa  
11 City, IA, USA}

12 [4]{Department of Physics and Materials Science, Faculty of Science, Chiang Mai University,  
13 Chiang Mai, Thailand}

14 [5]{Department of Statistics, Faculty of Science, Chiang Mai University, Chiang Mai,  
15 Thailand}

16 Correspondence to: T. Amnuaylojaroen (tum@ucar.edu), M. C. Barth (barthm@ucar.edu)

17

18

## 1 **Abstract**

2 In order to improve our understanding of air quality in Southeast Asia, the anthropogenic  
3 emissions inventory must be well represented. In this work, we apply different anthropogenic  
4 emission inventories in the Weather Research and Forecasting Model with Chemistry (WRF-  
5 Chem) version 3.3 using MOZART gas-phase chemistry and GOCART aerosols to examine  
6 the differences in predicted carbon monoxide (CO) and ozone (O<sub>3</sub>) surface mixing ratios for  
7 Southeast Asia in March and December 2008. The anthropogenic emission inventories  
8 include the Reanalysis of the TROpospheric chemical composition (RETRO), the  
9 Intercontinental Chemical Transport Experiment-Phase B (INTEX-B), the MACCity  
10 emissions (adapted from the Monitoring Atmospheric Composition and Climate and megacity  
11 Zoom for the Environment projects), the Southeast Asia Composition, Cloud, Climate  
12 Coupling Regional Study (SEAC4RS) emissions, and a combination of MACCity and  
13 SEAC4RS emissions. Biomass burning emissions are from the Fire Inventory from NCAR  
14 (FINNv1) model. WRF-chem reasonably predicts the 2-m temperature, 10-m wind, and  
15 precipitation. In general, surface CO is underpredicted by WRF-Chem while surface O<sub>3</sub> is  
16 overpredicted. The NO<sub>2</sub> tropospheric column predicted by WRF-Chem has the same  
17 magnitude as observations, but tends to underpredict NO<sub>2</sub> column over the equatorial ocean  
18 and near Indonesia. Simulations using different anthropogenic emissions produce only a slight  
19 variability of O<sub>3</sub> and CO mixing ratios, while biomass burning emissions add more  
20 variability. The different anthropogenic emissions differ by up to 30% in CO emissions, but  
21 O<sub>3</sub> and CO mixing ratios averaged over the land areas of the model domain differ by ~4.5%  
22 and ~8%, respectively, among the simulations. Biomass burning emissions create a  
23 substantial increase for both O<sub>3</sub> and CO by ~29% and ~16%, respectively, when comparing  
24 the March biomass burning period to December with low biomass burning emissions. The  
25 simulations show that none of the anthropogenic emission inventories are better than the  
26 others for predicting O<sub>3</sub> surface mixing ratios. However, the simulations with different  
27 anthropogenic emission inventories do differ in their predictions of CO surface mixing ratios  
28 producing variations of ~30% for March and 10-20% for December at Thai surface  
29 monitoring sites.

30

## 1 **1 Introduction**

2 Southeast Asia, which includes the Indochina peninsula and the Indonesian archipelago, can  
3 have significant air quality problems. Understanding the contribution of different sources of  
4 tropospheric ozone ( $O_3$ ) and its precursors, carbon monoxide (CO) and nitrogen oxides ( $NO_x$   
5 =  $NO + NO_2$ ), for Southeast Asia provides valuable information on maintaining good air  
6 quality for both human well-being and ecosystems. Previous studies examining air pollutants  
7 and their sources via regional model simulations have focused primarily on China (e.g. Wang  
8 et al., 2005; Geng et al., 2011), East Asia (Han et al., 2008; Tanimoto et al., 2009), and India  
9 (Adhikary et al., 2007; Kumar et al., 2012; Ghude et al., 2013). Here, we examine the effect  
10 of different emission inventories on modeled surface  $O_3$  and CO for Southeast Asia, a region  
11 generally ignored in previous studies.

12 Previous studies have indicated that both local anthropogenic and biomass burning emissions,  
13 as well as emissions upstream are important for local  $O_3$  air quality in Asia. In East Asia,  
14 Tanimoto et al. (2009) noted relatively small changes in decadal  $O_3$  trends at sites near the  
15 Japanese coast, but a larger increase in measured  $O_3$  at a remote mountainous site in Japan.  
16 Using a regional chemistry transport model, Tanimoto et al. (2009) attributed half of the  
17 observed increase at the mountainous site to increasing anthropogenic emissions in Asia. The  
18 results from this study suggested that the actual growth in emissions between 1998-2007 was  
19 significantly underestimated. Using a nested eastern Asia domain within a global chemistry  
20 transport model, Wang et al. (2011) found that local sources of  $O_3$  precursors produced much  
21 of the  $O_3$  in the region; however,  $O_3$  transported from Europe, North America, India and  
22 Southeast Asia also impacted  $O_3$  concentrations in eastern China depending on the season.  
23 Liu et al. (2008), using a regional air quality model, determined that fossil fuel and biomass  
24 burning emissions from East Asia increased surface CO and  $O_3$  in Taiwan by 70-150% and  
25 50-100%, respectively, compared to model results that excluded background emissions. They  
26 attributed up to 20% of the surface CO and  $O_3$  in Taiwan to biomass burning emissions from  
27 Eastern China. Both the aerosol optical depth and  $O_3$  concentrations in the Pearl River Delta  
28 were also found to be affected by biomass burning emissions occurring upstream in Southeast  
29 Asia (Deng et al., 2008).

30 Southeast Asia is subject to the effluent of pollution from the main continent, yet the region  
31 itself is rapidly growing and has increasing anthropogenic and biomass burning emissions,  
32 which are especially high during the dry season (November-April). To simulate  $O_3$  production

1 and concentrations in Southeast Asia, realistic estimates of emissions from both local and  
2 regional sources, including fossil fuel use, other anthropogenic activities, and biomass  
3 burning, must be available. Emission inventories for Asia have been developed by several  
4 groups (e.g., Akimoto and Narita, 1994; Streets et al., 2003; Ohara et al., 2007; Zhang et al.,  
5 2009; Kurokawa et al., 2013) for both chemistry-climate and air quality studies. For example,  
6 the REanalysis of the TROpospheric chemical composition (RETRO) and the Emission  
7 Database for Global Atmospheric Research (EDGAR) emissions inventories (Olivier et al.,  
8 2005; Schultz et al., (2007)) are global emissions inventories developed for chemistry-climate  
9 studies. Streets et al. (2003) developed a 2001 emission inventory for the ACE-Asia (Asian  
10 Pacific Regional Aerosol Characterization Experiment) and TRACE-P (Transport and  
11 Chemical Evolution over the Pacific) field campaigns that took place in the East Asian and  
12 Western Pacific region during spring 2001. Zhang et al. (2009) developed a 2006 emissions  
13 inventory for Asia to support the Intercontinental Chemical Transport Experiment-Phase B  
14 (INTEX-B) field campaign. The INTEX-B field campaign emphasized China emissions  
15 because they dominate the Asia pollutant outflow to the Pacific. Ohara et al. (2007) developed  
16 the Regional Emission inventory in Asia (REAS) for 1980-2020 in order to conduct air  
17 quality studies for recent past, present day, and near future time periods. More recently,  
18 Kurokawa et al. (2013) released REAS version 2.1, providing updated emissions for each year  
19 from 2000 to 2008 for Asian countries east of  $\sim 55^{\circ}\text{E}$ . The MACCity emissions inventory  
20 (Granier et al., 2011), which is an outcome from two European Commission projects (MACC  
21 and CityZen), is a 1980-2010 global emissions inventory for chemistry-climate studies. Most  
22 recently the Southeast Asia Composition, Clouds and Climate Coupling by Regional Study  
23 (SEAC4RS) emissions inventory (Lu and Street, 2012) for 2012 emissions has been released  
24 for field campaign support. Four emission inventories, RETRO, INTEX-B, MACCity and  
25 SEAC4RS, will be described in more detail in section 3.

26 While previous studies (e.g. Ohara et al., 2007) have compared different emission inventories,  
27 a comparison of simulated surface CO and O<sub>3</sub> mixing ratios resulting from different emission  
28 inventories, yet using the same model framework, has not been done. Here, the Weather and  
29 Forecasting Model coupled with Chemistry (WRF-Chem) is used to examine the variability of  
30 predicted O<sub>3</sub> and CO surface mixing ratios when five different anthropogenic emission  
31 inventories (RETRO, INTEX-B, MACCity, SEAC4RS and a modified SEAC4RS) are used  
32 as inputs. By conducting this comparison using the same model, differences in results due to  
33 model meteorology are mitigated. We focus this study on Southeast Asia, an area that has

1 received little attention, yet has substantial anthropogenic and biomass burning emissions. As  
2 part of our study, we examine the effect of biomass burning emissions on surface O<sub>3</sub> and CO  
3 by the contrasting results from a low biomass-burning period (December) with a high  
4 biomass-burning period (March).

5 We begin this manuscript by describing the model configuration (Section 2) and emission  
6 inventories (Section 3) applied in the model simulations. We then evaluate the model results  
7 (Section 4) with available datasets. In Section 5, we compare the surface O<sub>3</sub> and CO  
8 predictions among the different simulations in order to quantify the variability produced by  
9 the different emission inventories.

## 10 **2 Model Description and Configuration**

11 We use the Weather Research Forecasting Model (Skamarock et al., 2008) coupled with  
12 Chemistry (WRF-Chem version 3.3) to investigate the variation of O<sub>3</sub> and CO predictions  
13 among different anthropogenic emissions inventories for Southeast Asia. The WRF-Chem  
14 model is a new-generation regional air quality model (Grell et al., 2005; Fast et al., 2006) that  
15 shares the meteorology and chemistry routines, the same land surface schemes, time-transport  
16 schemes, vertical mixing parameterizations, and time steps for transport and vertical mixing.

17 For this study, one model domain was configured to cover the entire area of Southeast Asia  
18 (SEA) and a part of China and India (Figure 1). The model was run with a horizontal grid  
19 spacing of 36 km and 51 vertical levels from the surface to 10 hPa. The vertical grid spacing  
20 stretched from ~60 m near the surface to ~700 m near the tropopause. The initial and  
21 boundary conditions were from NCEP Final Analysis (FNL) 1° × 1° data for meteorological  
22 variables, which include winds, potential temperature, pressure, and water vapor. These  
23 variables and condensed water (i.e., cloud particles), and chemistry species were integrated  
24 forward in time using a Runge-Kutta integration method. The moisture variables and  
25 chemistry species were advected using a monotonic scheme (Wang et al., 2009). Grid  
26 nudging (Stauffer and Seaman, 1990) was employed for the horizontal wind, temperature and  
27 water vapor for all vertical levels to ensure the accuracy of the large-scale meteorology during  
28 the month of simulation. The nudging coefficients for all variables were set to be 0.0003 s<sup>-1</sup>,  
29 and nudging was performed every 6 hours, consistent with the timing of the FNL data.

30 The model set-up used the following modules and parameterizations. Cloud physics was  
31 represented by the Thompson et al. (2004) parameterization, which predicts the mass mixing

1 ratio for rain, snow, and graupel and mass and number of cloud water and cloud ice. The  
2 Grell-3 scheme, based on the Grell and Devenyi (2002) scheme, was used for the  
3 parameterization of sub-grid convection. The planetary boundary layer was parameterized  
4 with the Mellor-Yamada-Janjic (MYJ) scheme (Janjic, 2002) and the Noah land surface  
5 model (Chen and Dudhia, 2001) was used to provide heat and moisture fluxes over land. For  
6 heating rates, the Goddard scheme (Chou and Suarez, 1994) was used for short wave radiation  
7 and the Rapid Radiative Transfer Model (Mlawer et al., 1997) was used for long wave  
8 radiation. Feedbacks between aerosols and the radiation scheme were not included in any  
9 simulations.

10 The model is integrated for a 6 ½ week period. The first 2 weeks are for spinning up the  
11 model from the initial conditions to a state that is primarily affected by the emissions. Initial  
12 and boundary conditions for the chemical species were provided by the global chemistry  
13 Model for Ozone and Related Chemical Tracers, version 4 (MOZART4; Emmons et al.,  
14 2010) 6-hourly output. MOZART4 includes 84 gas-phase species, 12 bulk aerosol  
15 compounds, 39 photolysis and 127 gas-phase reactions. In our WRF-Chem simulations, gas-  
16 phase chemistry was represented by the MOZART chemistry mechanism and aerosols by the  
17 GOCART representation (Chin et al., 2000). A kinetic pre-processor and Rosenbrock solver  
18 (Sandu et al., 2006) was applied. The photolysis rates were computed using fast-TUV (Tie et  
19 al., 2003), which modifies the photolysis rates based on the presence of aerosols and clouds in  
20 each model grid cell. Dry deposition of gases and aerosols followed the Wesely (1989)  
21 resistance method. Wet deposition of soluble gases was calculated using the method described  
22 by Neu and Prather (2012).

23 Emissions from biomass burning, undisturbed vegetation, and anthropogenic sources were  
24 included in the simulations. The Fire Inventory from NCAR (FINN) model (Wiedinmyer et  
25 al., 2010) provided daily, 1 km resolution, global estimates of trace gas and particulate  
26 emissions from open burning including wildfires, agricultural fires, and prescribed burning  
27 for all the simulations conducted. Biofuel use and trash burning were not included in the  
28 FINN emission estimates. Biogenic emissions were computed online by the Model of  
29 Emissions of Gases and Aerosols from Nature (MEGAN) Version 2.04 (Guenther et al.,  
30 2006), which uses WRF-predicted temperature and downward radiation for its calculations.  
31 The anthropogenic emission inventories used as inputs to the WRF-Chem simulations are  
32 described in Section 3.1.

### 1 **3 Emissions**

2 In this study we perform WRF-Chem simulations with four different anthropogenic emission  
3 inventories, consisting of RETRO, INTEX-B, MACCity and SEAC4RS, and an inventory  
4 combining MACCity and SEAC4RS emissions. The simulations also include biogenic  
5 emissions (MEGAN v2.04) and biomass burning (FINNv1) emissions, which were the same  
6 in all simulations. Different groups have compiled the different anthropogenic emission  
7 inventories for different years: RETRO for 2000, INTEX-B for 2006, MACCity for 2010 and  
8 SEAC4RS for 2012. The emission inventories have in common several sectors contributing to  
9 the emissions (Table 1), but there are some sectors not included in one or two inventories that  
10 are detailed below. Due to these differences, the total emissions and associated uncertainties  
11 for the region are variable. The five emission inventories were applied to 1) evaluate surface  
12 CO and O<sub>3</sub> predictions with monitoring station observations, and 2) determine the extent the  
13 model predictions are limited by variations in the emissions inventories.

#### 14 **3.1 Description of the Anthropogenic Emission Inventories**

15 The RETRO project aimed at analyzing the long-term changes in the atmospheric budget of  
16 trace gases and aerosols over the time period from 1960 to 2000. The RETRO anthropogenic  
17 emissions (Schultz et al., 2007) are derived from a preliminary version of the TNO  
18 (Netherlands Organization for Applied Scientific Research) emissions, for the 1960–2000  
19 time period with spatial resolution of 0.5° x 0.5°. The anthropogenic emissions in the RETRO  
20 inventory include mainly combustion sources (Granier et al., 2011), but solvent use and other  
21 industrial processes are included (Table 1). Schultz et al. (2007) report several uncertainties  
22 associated with the RETRO emissions. These uncertainties include omission of specific  
23 sectors (e.g. railway traffic or cement manufacturing), underestimation of CO combustion  
24 emissions and NO<sub>x</sub> ship traffic emissions, and the lack of weekly and diurnal profiles of  
25 emissions. For the Southeast Asia region the RETRO seasonal cycle is based on the LOTUS-  
26 EUROS European monthly pattern (Schaap et al., 2005; which is derived from a critical  
27 review of the monthly variation by emission sector), but has a reduced amplitude. Kurokawa  
28 et al. (2013) show that there is very little seasonal cycle for anthropogenic emissions of NO<sub>x</sub>  
29 and black carbon over India, which is a region similar to Southeast Asia in terms of climate.  
30 The RETRO inventory provided regional information for the emissions of a variety of non-  
31 methane volatile organic compounds (NMVOCs) including ethane, propane, butanes,  
32 pentanes, hexanes and higher alkanes, ethene, propene, ethyne, other alkenes and alkynes,

1 benzene, toluene, xylene, trimethyl benzenes and other aromatics, organic alcohols, esters,  
2 ethers, chlorinated hydrocarbons, formaldehyde and other aldehydes, ketones, organic acids,  
3 and other VOCs.

4 As part of the INTEX-B field campaign, which was conducted by the National Aeronautics  
5 and Space Administration (NASA) in spring 2006, anthropogenic emissions were developed  
6 for the specific year and season as the field campaign (Zhang et al., 2009). The emissions are  
7 estimated for eight major chemical species, sulfur dioxide (SO<sub>2</sub>), NO<sub>x</sub>, CO, NMVOCs, PM<sub>10</sub>,  
8 PM<sub>2.5</sub>, black carbon (BC) and organic carbon (OC), with a spatial resolution of 0.5° x 0.5°.  
9 To represent the individual VOCs represented in the MOZART mechanism, the NMVOC  
10 emissions are speciated based on the ratios of the individual VOC to the total NMVOCs  
11 derived from the RETRO inventory. That is, the individual VOC fraction from the RETRO  
12 inventory is multiplied with the total INTEX-B NMVOC to get the individual VOC  
13 emissions. The INTEX-B emissions contain four major sectors (Table 1), power generation,  
14 industry, residential, and transportation. The uncertainty of the INTEX-B emissions for the  
15 Southeast Asian countries is estimated to be similar to the TRACE-P emissions uncertainty  
16 (Zhang et al., 2009), e.g. +/-37% for NO<sub>x</sub> emissions and +/-185% for CO emissions. The  
17 INTEX-B emissions uncertainties for China are smaller (+/-31% for NO<sub>x</sub> and +/-70% for  
18 CO).

19 The MACCcity emissions (Granier et al., 2011) are an outcome of two European Commission  
20 projects, MACC (Hollingsworth et al. 2008) and CityZen (<http://cityzen-project.eu>) and are  
21 an extension of the ACCMIP historical emissions dataset (Lamarque et al., 2010). The goal of  
22 the MACCcity emissions inventory is to support the IPCC-AR5 (Intergovernmental Panel for  
23 Climate Change Assessment Report 5), providing historical emissions from a variety of  
24 emission sectors (Table 1) on a decadal basis from 1960 to 2020, as well as for future  
25 emissions scenarios based on RCPs (Representation Concentration Pathways; van Vuuren et  
26 al., 2011). Anthropogenic emissions have been interpolated on a yearly basis between the  
27 base years 1990, 2000, 2005 and 2010. The MACCcity emissions are estimated for 19  
28 chemical species: CO, ethane, ethene, propane, propene, butane and higher alkanes, butene  
29 and higher alkenes, methanol, other alcohols, formaldehyde, other aldehydes, acetone, other  
30 ketones, total aromatics, ammonia, NO<sub>x</sub>, SO<sub>2</sub>, BC, and OC, with spatial resolution of 0.5° x  
31 0.5°. Because the 2000 MACCcity emissions inventory does not have substantial biases  
32 compared to other emissions inventories, it is expected that the 2010 MACCcity emissions



1 inventory has uncertainties similar to those discussed by Lamarque et al. (2010) who did not  
2 find significant biases in their comparison of 2000 MACCity emissions with published  
3 emission estimates (e.g. RETRO and EDGAR). However, they estimate that these emissions  
4 have an uncertainty of about a factor of 2 based on Bond et al. (2004, 2007) and Smith et al.  
5 (2010). The uncertainty of the 2010 emissions was not reported. In this study, we use the  
6 2010 emissions estimates from MACCity, which are based on the RCP8.5 scenario.

7 The SEAC4RS emissions inventory (Lu and Street, 2012) is a regional anthropogenic  
8 emission dataset prepared for the NASA SEAC4RS field campaign and for the Asia region,  
9 represents an update of the TRACE-P emissions (Streets et al., 2003). These emissions are  
10 appropriate for year 2012 and include four emissions sectors: residential, industry, power and  
11 transportation (Table 1). There are 10 major chemical species, CH<sub>4</sub>, CO, NO<sub>x</sub>, NMVOC, CO<sub>2</sub>,  
12 SO<sub>2</sub>, PM<sub>10</sub>, PM<sub>2.5</sub>, BC and OC, with spatial resolution of 0.1° x 0.1°. Not only does this  
13 emissions inventory provide a finer resolution than the other inventories applied in this study,  
14 the SEAC4RS emissions data include an update of the Asia emission estimates using new  
15 energy use data and updated emission factors (both reflecting the year 2012), as well as the  
16 development of a new emission inventory for Southeast Asia using a technology-based  
17 methodology, which is the first detailed emission update for the region since TRACE-P.  
18 Similar to the INTEX-B inventory described above, the total NMVOC emissions were  
19 speciated to the individual VOC species of the MOZART-4 mechanism using fractions  
20 derived from the RETRO inventory.

21 In addition to the four inventories described above, we have conducted a simulation with a  
22 combined MACCity/SEAC4RS emissions inventory, which replaces MACCity with the  
23 SEAC4RS emissions over Asia yet includes the MACCity ship emissions, which include  
24 international shipping, domestic shipping and fishing. Note, that in the RETRO and INTEX-B  
25 inventories, ship emissions represent only international shipping. The ship emissions for  
26 RETRO, INTEX-B, and MACCity are listed in Table 2. In the MACCity emissions inventory,  
27 ship emissions account for 15% of the NO emissions and 0.8% of the CO emissions. To  
28 ensure consistency in the MACCity/SEAC4RS simulation, the SEAC4RS emissions have  
29 been regridded from 0.1° x 0.1° resolution to 0.5° x 0.5°. This regridding causes differences  
30 between the SEAC4RS-only and MACCity/SEAC4RS emissions outside the shipping regions  
31 in the model domain.

1 While both the RETRO and MACCcity emission inventories have monthly temporal  
 2 variability, the INTEX-B and SEAC4RS inventories are annual totals. A monthly profile was  
 3 created from the RETRO emissions. The MACCcity seasonal variation is very similar to  
 4 RETRO for CO emissions, but does differ somewhat for NO emissions. The change of NO  
 5 emissions from February (when we start the simulation) to March differs between these two  
 6 inventories with little change in high NO emissions for the MACCcity inventory and a 5%  
 7 decrease in NO emissions for the RETRO inventory. While this is a small difference, the  
 8 change in NO emissions could affect O<sub>3</sub> production downwind of NO sources. To obtain the  
 9 monthly profile for INTEX-A and SEAC4RS emissions, the fraction of the annual emissions  
 10 assigned to each month ( $Frac_{Monthly}$ ) was calculated from the ratio of the RETRO monthly  
 11 emissions ( $RETRO_{Monthly}$ ) to the RETRO annual emissions ( $RETRO_{Annual}$ ). The monthly  
 12 fraction was then multiplied by the annual emissions of both the INTEX-B and SEAC4RS  
 13 inventories to estimate the monthly emissions. This procedure is described by the following  
 14 equations:

$$15 \quad RETRO_{Annual} = \sum_{i=1}^{12} RETRO_{Monthly} \quad (1)$$

$$16 \quad Frac_{Monthly}(i) = \frac{RETRO_{Monthly}(i)}{RETRO_{Annual}} \quad (2)$$

$$17 \quad Emission_{Monthly}(i) = Frac_{Monthly}(i) \times Emission_{Annual} \quad (3)$$

18 where the  $Emission_{Monthly}$  is the monthly emissions for the INTEX or SEAC4RS inventory and  
 19  $Emission_{Annual}$  is the annual emissions from the INTEX or SEAC4RS inventory.

## 20 **3.2 Emission Comparison**

21 The monthly emissions from the five different anthropogenic emissions inventories and the  
 22 biomass burning emissions calculated by the FINN model for CO and NO<sub>x</sub> are compared for  
 23 both March and December in Figures 1 – 4. The sum of these emissions over the entire model  
 24 domain is listed in Table 2. In March, the biomass burning sources dominate the emissions of  
 25 CO. The biomass burning occurs primarily over the Indochina peninsula and Southeast China  
 26 where CO biomass emissions dominate the inventory. In March in Southeast Asia, ~70% of  
 27 the total CO emissions is from biomass burning and only ~30% is from anthropogenic  
 28 emissions. This partitioning is true for all the emission inventories applied in this study. In  
 29 December, the biomass burning emissions are much smaller.

1 Anthropogenic emissions of CO vary between emissions inventories, with RETRO and  
2 MACCity emissions having higher values, particularly in northeast India and southeast China.  
3 Over the entire domain, the anthropogenic NO<sub>x</sub> emissions are quite similar between RETRO,  
4 INTEX-B, MACCity, and MACCity/SEAC4RS emissions, but are much smaller in the  
5 SEAC4RS inventory, since this inventory alone does not include ship emissions. By  
6 comparing RETRO emissions to MACCity/SEAC4RS emissions, the total anthropogenic  
7 emissions in Southeast Asia decreased by ~30% for CO and ~13% for NO between 2000 and  
8 2012 with 2010 ship emissions.

9 Comparison of the total CO emissions from the various inventories across Southeast Asia  
10 (Table 2) show that in March, the RETRO inventory is within +/- 5% of the INTEX-B and  
11 MACCity inventories, but is ~20% greater than the MACCity/SEAC4RS and SEAC4RS  
12 inventories. In December, the CO MACCity/SEAC4RS inventory is 35% lower than the  
13 RETRO emissions inventory. The SEAC4RS NO emissions are substantially less (~45%)  
14 than the other inventories in both March and December because of the lack of ship emissions  
15 in the SEAC4RS inventory. NO emissions in the INTEX-B and MACCity inventories are  
16 similar to each other and ~10% lower than the RETRO emissions. In December, the INTEX-  
17 B, MACCity and MACCity/SEAC4RS NO emissions are similar and are ~25% lower than  
18 the RETRO inventory.

19 The CO and NO emissions used in our study are larger than the REAS v1 emissions (Ohara et  
20 al., 2007) for our modeling domain (Table 2). The REAS v1 estimate in Table 2 comes from  
21 the Emissions of atmospheric Compounds & Compilation of Ancillary Data (ECCAD) web  
22 site (<http://eccad.sedoo.fr>) to obtain emission estimates for the same region as our model  
23 domain, which encompasses small regions of India and China that are not included in the  
24 Southeast Asia region denoted by Ohara et al. (2007). For our model domain the REAS v1  
25 annual emissions are 91.4 Tg year<sup>-1</sup> for CO and 4.81 Tg year<sup>-1</sup> for NO<sub>x</sub>. For the Southeast  
26 Asia region, Ohara et al. (2007) report in their Table 6 annual CO and NO<sub>x</sub> emissions of 54.5  
27 and 3.77 Tg year<sup>-1</sup>, respectively, but these exclude international aviation, international  
28 shipping and open biomass burning. The REAS v1 emissions are even greater than the  
29 TRACE-P, EDGAR 3.2, and IIASA CO emissions (34.0, 42.6, 39.8 Tg CO year<sup>-1</sup>,  
30 respectively) but are more similar to TRACE-P, EDGAR 3.2, and IIASA NO<sub>x</sub> emissions  
31 (3.06, 3.91, 3.94 Tg NO<sub>x</sub> year<sup>-1</sup>, respectively) for Southeast Asia (Ohara et al., 2007) as well  
32 as REAS v2.1 (Kurakawa et al., 2013), which were 36.2 Tg CO year<sup>-1</sup> and 3.00 Tg NO<sub>x</sub> year<sup>-1</sup>.

1 Thus, the emissions used here are larger than the REAS emissions inventories as well as other  
2 previous inventories.

3

#### 4 **4 Data Used for the Model Evaluation**

5 To evaluate the ability of the WRF-Chem model to represent the meteorology and chemical  
6 composition over Southeast Asia during March and December 2008, the model results are  
7 evaluated with observations. The data used for the model evaluation is described here.

#### 8 **4.1 Meteorology Data Description**

9 The predicted meteorology from the WRF simulations, which is the same for all model  
10 simulations, was evaluated by comparing 2-m temperature, 10-m winds, and precipitation  
11 with existing observations. The observations used for this evaluation include the Modern-Era  
12 Retrospective Analysis For Research And Applications (MERRA) products, the Tropical  
13 Rainfall Measuring Mission (TRMM) satellite data, and data from the Global Precipitation  
14 Climatology Center (GPCC).

15 The MERRA product (Rienecker et al., 2011) is generated using Version 5.2.0 of the GEOS-5  
16 DAS (Goddard Earth Observing System Model Data Assimilation System) with the model  
17 and analysis each at about  $0.5^\circ \times 0.6^\circ$  resolution. MERRA has complete analysis of over 30  
18 years (from 1979 to present) of data. The 2-m temperature and 10-m winds produced by the  
19 MERRA analysis system are hourly. However, the provided monthly-averaged data were  
20 used here to evaluate the WRF results.

21 The main objective of TRMM satellite (Huffman et al., 1997), which is a joint mission  
22 between the National Aeronautics and Space Administration (NASA) and Japan Aerospace  
23 Exploration Agency (JAXA), is to monitor rainfall in the tropics. We compare the WRF-  
24 Chem monthly surface rainfall to the TRMM product that is a combination of instruments,  
25 including the Precipitation Radar and TRMM Microwave Imager, allowing us to compare  
26 model results with the high-resolution data from the Precipitation Radar filled in by data from  
27 the TRMM Microwave Imager. The precipitation gauge analysis is used to correct any biases  
28 in the satellite data (Huffman and Bolvin, 2012).

29 Monthly precipitation from the GPCC dataset (Rudolf et al., 2005a,b) is obtained from global  
30 station data that is gridded onto a  $1^\circ \times 1^\circ$  global domain. The GPCC monthly precipitation

1 product is based on anomalies from the climatological mean at each station. The anomalies  
2 are spatially interpolated by using a modified version of the robust empirical interpolation  
3 method SPHEREMAP. The method constitutes a spherical adaptation (Willmott et al., 1985)  
4 of Shepard's empirical weighting scheme (Shepard, 1968; Schneider et al., 2011).

## 5 **4.2 Chemistry Data Description**

6 Observations from four measurement platforms are used to evaluate the WRF-Chem  
7 predictions of CO, O<sub>3</sub> and NO<sub>2</sub>: a ground-based monitoring network in Thailand, ozonesondes  
8 in the Southeast Asia region, Version 6 Measurement of Pollution In the Troposphere  
9 (MOPITT) satellite instrument, and the Ozone Monitoring Instrument (OMI) satellite  
10 instrument. The ground-based chemistry observations in Thailand are provided by the Thai  
11 Pollution Control Department (PCD). The Thai PCD monitors the hourly surface  
12 concentrations of five chemical species: O<sub>3</sub>, CO, NO<sub>2</sub>, SO<sub>2</sub> and PM<sub>10</sub> at six locations (Figure  
13 5g). The measurement sites in Thailand are located in urban areas and therefore are dominated  
14 by urban (especially motor vehicles) emissions. These data are measured by using the  
15 "reference method" or "equivalent methods". Almost all O<sub>3</sub> observation instruments are from  
16 Teledyne Advanced Pollution Instrumentation Model 400 ([http://www.teledyne-](http://www.teledyne-api.com/products/400e.asp)  
17 [api.com/products/400e.asp](http://www.teledyne-api.com/products/400e.asp)). The instrument has a lower detection limit of 0.6 ppbv and a  
18 precision of 1%. Almost all CO observation instruments are from Teledyne Advanced  
19 Pollution Instrumentation Model 300 (<http://www.teledyne-api.com/products/300e.asp>),  
20 which has a lower detection limit of 40 ppbv and a precision of 0.5%. The PCD  
21 measurements periodically have missing data, but the missing data are only ~15% of the time.

22 The SHADOZ ozonesonde network (Thompson et al., 2012) was initiated to provide vertical  
23 profiles of O<sub>3</sub> in the tropics for satellite data verification, model evaluation, and insights into  
24 tropical chemistry and dynamics. SHADOZ has collected more than 3000 O<sub>3</sub> profiles from 14  
25 sites in tropical and subtropical regions using balloon-borne electrochemical concentration  
26 cell (ECC) O<sub>3</sub> detectors flown with standard radiosondes. It is estimated that the accuracy  
27 and precision of the O<sub>3</sub> measurement is 5%, but biases can be found with individual stations.  
28 Ozonesondes from three stations, Kuala Lumpur, Malaysia, Hanoi, Vietnam, and Watukosek,  
29 Java (Figure 5g), are used in the model evaluation presented in this manuscript. Total O<sub>3</sub>  
30 column at these stations can be 5-10% lower than total O<sub>3</sub> measured by the OMI satellite  
31 instrument (Thompson et al., 2012).

1 Satellite observations are quite valuable for model evaluation, but require careful  
2 interpretation to be used quantitatively. In many cases (as in MOPITT CO and OMI NO<sub>2</sub>) the  
3 retrieved mixing ratios or column densities can be expressed as a linear combination of the  
4 true atmospheric profile ( $x$ ) and a priori information ( $x_a$ ), balanced according to the averaging  
5 kernels ( $A$ ) ( $I$  is the identity matrix):

$$6 \quad x_{\text{ret}} = \mathbf{A}x + (\mathbf{I} - \mathbf{A})x_a \quad (4)$$

7 The averaging kernels represent the sensitivity of the retrievals to the actual concentration  
8 profiles, and vary in time and space depending on the temperature profile, the thermal contrast  
9 between air and surface temperatures, the concentration profile and surface emissivity.

10 The new versions of MOPITT data (Versions 5 & 6; Deeter et al. 2011; 2012; 2013; Worden  
11 et al. 2010), which we used in this paper, have improved near surface CO retrievals over  
12 Version 4. The V6 MOPITT uses both near-infrared and thermal-infrared observations  
13 simultaneously to enhance the retrieval sensitivity of CO in the lower troposphere. This  
14 feature is important to air quality analyses and studies of CO sources. The V5 MOPITT  
15 surface-level CO validation shows biases on the order of a few percent, and V6 is very similar  
16 (Deeter et al., 2012).

17 The OMI Level-3 Global Gridded NO<sub>2</sub> data product, archived at the NASA Goddard Earth  
18 Sciences Data and Information Service Center (GES DISC), has a spatial resolution of about  
19 13 km x 24 km at nadir in normal operational mode. OMI measures the backscattered  
20 radiation over the 0.27–0.5 μm wavelength range to obtain the total column of trace species,  
21 such as NO<sub>2</sub>, O<sub>3</sub>, formaldehyde, SO<sub>2</sub> and aerosols. The tropospheric NO<sub>2</sub> column retrieval  
22 algorithm follows Bucseila et al. (2006) who use the DOAS methodology, air mass factors,  
23 and typical NO<sub>2</sub> profiles from chemical transport models to obtain the vertical column  
24 density. The OMI tropospheric NO<sub>2</sub> column data have been shown to have a good correlation  
25 with INTEX-B aircraft measurements (Boersma et al., 2008). Good agreement of OMI  
26 tropospheric NO<sub>2</sub> column has also been found with MAX-DOAS ground-based measurements  
27 (Kramer et al., 2008). However, some recent studies have suggested that the OMI retrieval  
28 has a positive bias of 0–30% (e.g., Boersma et al., 2009; Zhou et al., 2009). To evaluate NO<sub>2</sub>  
29 from model results, we compare the tropospheric column of NO<sub>2</sub> from the OMI Level-3  
30 Global Gridded NO<sub>2</sub> data product with WRF-Chem NO<sub>2</sub> columns that have been adjusted  
31 using the averaging kernel and a priori information (following equation 4) provided with the  
32 data product (e.g., Emmons et al., 2004).

1

## 2 **5 Model Results and Evaluation**

### 3 **5.1 Meteorology Evaluation**

4 Monthly-averaged 2-m temperature, wind speed and direction are compared to the MERRA  
5 reanalysis dataset. In general, the model-predicted temperature agrees well with the MERRA  
6 output (Figure 5) for the March 2008 simulation, although some regions, e.g. Indochina  
7 peninsula, have 2-3°C lower temperatures than the monthly-averaged reanalysis output. The  
8 WRF-predicted wind speed pattern is similar to the MERRA output for March. However, the  
9 wind speed is over-predicted in the South China Sea by  $\sim 2 \text{ m s}^{-1}$ . The wind direction agrees  
10 quite well with MERRA output (Figure 5e,f). For December 2008 (not shown), the simulated  
11 2-m temperature, 10-m wind speed and wind direction, in general, also agree well with the  
12 MERRA output; however, the temperature is slightly under-predicted over land and the wind  
13 speed is over-predicted over the South China Sea. The low bias in temperature and high bias  
14 in wind speed can impact the prediction of chemical species mixing ratios. For example, the  
15 chemical reactions likely will proceed at a slightly lower rate (because of their dependence on  
16 temperature) resulting in formation of products further away from the source. Additionally,  
17 biogenic emissions may be underpredicted, since these emissions increase with increasing  
18 temperatures and a low bias in temperature can lead to lower emissions.

19 WRF reasonably predicts the precipitation pattern in March (Figure 6a-c) when compared to  
20 TRMM and GPCC data. Low precipitation is observed over the coast of Burma, the northern  
21 part of the South China Sea, and the tip of the Indochina peninsula, and high precipitation is  
22 predicted near the equator over the oceans, Malaysian peninsula, and Indonesia. However, the  
23 WRF results overestimate precipitation near the equator by 10 to 100 mm for March. In  
24 December (Figure 6d-f), WRF also over-predicts the magnitude of precipitation over the  
25 water, but shows reasonable agreement north of 10N especially over land. The precipitation in  
26 this region is dominated by rain from convection, which controlled by mesoscale processes.  
27 The WRF simulations presented here have a 36 km horizontal resolution, and at this  
28 resolution, the model relies on a cumulus parameterization to produce the rain. Due to the  
29 coarse model resolution for a region with plenty of tropical convection, a situation which is  
30 notoriously difficult to represent in models, the poor prediction of precipitation near the  
31 equator is not unexpected. Koo and Hong (2010) also found oceanic convection to be

1 overpredicted by the WRF model. However, over land, where the chemical predictions of this  
2 study are evaluated, the WRF precipitation has better agreement with observations. As a  
3 consequence of the higher precipitation predicted by WRF, WRF-chem may overpredict the  
4 removal of soluble trace gases (e.g. nitric acid), thereby affecting the photochemistry in the  
5 region.

## 6 **5.2 Evaluation of Chemistry**

### 7 **5.2.1 Ensemble Surface Means and Variations**

8 To show the distribution of the monthly-mean surface mixing ratios for CO, O<sub>3</sub>, and NO<sub>x</sub> in  
9 March and December, the WRF-Chem results from all five simulations (with different  
10 emissions inventories) have been averaged giving an ensemble mean (Figure 7). In general,  
11 surface-level CO and NO<sub>x</sub> mixing ratios have highest values over the land regions and lowest  
12 values over the ocean near the equator. By comparing the model results from March (high  
13 biomass burning emissions) to those from December (low biomass burning emissions), the  
14 influence of biomass burning emissions can be seen for all three species. CO mixing ratios are  
15 > 500 ppbv over Burma and northern Thailand during March compared to 200-500 ppbv  
16 during December.. Monthly-averaged O<sub>3</sub> mixing ratios, which reach 70-90 ppbv, are largest  
17 during March over the regions where biomass burning is occurring and downwind of these  
18 emissions. With a shorter lifetime, high NO<sub>x</sub> mixing ratios of 4-30 ppbv are confined to  
19 regions close to the NO<sub>x</sub> sources.

20 The variation, which is defined as the standard deviation of the five simulations, in the  
21 predicted monthly-averaged surface mixing ratios of CO, O<sub>3</sub>, and NO<sub>x</sub> across the five  
22 simulations is highlighted in Figure 8. Because we conducted each simulation with the same  
23 meteorology and biomass burning emissions, the primary cause for the variations are the  
24 differences in the anthropogenic emissions. CO mixing ratios vary across simulations by  
25 <20%, but variations of ~30-60% are found near Bangladesh and Indonesia for both March  
26 and December. O<sub>3</sub> mixing ratios have up to 30% variation near the tip of the Malaysian  
27 peninsula and near Indonesia, but have much smaller variability elsewhere. Mixing ratios of  
28 NO<sub>x</sub> have the most variation among the simulations. The 70-100% variations for NO<sub>x</sub>,  
29 especially over the South China Sea, are from the differences in ship emissions from each  
30 inventory. There are also high NO<sub>x</sub> variations in several cities as seen by the locally high



1 values in Figure 8e,f, due to different emission strengths in each inventory and to missing  
2 emission sectors in some inventories (e.g. shipping emissions in the SEAC4RS inventory).

### 3 **5.2.2 CO Evaluation**

4 The 6-hourly daytime (00, 06, 12 UTC) CO mixing ratios from WRF-Chem with each of the  
5 five inventories are compared to observations from the six ground-site measurements: Chiang  
6 Mai (CM) in northwest Thailand, Khonkaen (KK) in eastern Thailand, Nonthaburi (NTB) in  
7 the Bangkok metropolitan region, Sarabuti (SRB) just north of Bangkok, Chonburi (CB)  
8 southeast of Bangkok, and Suratthani (SRT) in the southern peninsula (Figure 5g). These sites  
9 are located in urban environments with background conditions ranging from high biomass  
10 burning in northern Thailand to more marine conditions in southern Thailand. For March  
11 when biomass burning emissions are a large source of CO, the WRF-Chem simulations agree  
12 well with the monthly-mean mixing ratio for Chiang-Mai in northwest Thailand and Chonburi  
13 in southeast Thailand (Figure 9), with moderate correlation coefficients (Table 3) of  $r^2 = 0.48$   
14 to 0.51. However, WRF-chem generally underpredicts CO at the other stations, especially  
15 Nonthaburi. In December, the predicted 6-hourly daytime surface CO for all simulations is  
16 much less than the observations, with the exception of the Chonburi site. The large  
17 underprediction is reflected by the bias calculation (Table 4). Part of the underprediction is a  
18 result of the coarse model resolution (36 km), which cannot capture the highly variable  
19 emissions and high CO concentrations in an urban setting where the measurement site is  
20 located. However, the underprediction of CO could also be due to low anthropogenic  
21 emissions (discussed further in Section 5), a high planetary boundary layer height, which  
22 would cause dilution of surface mixing ratios, and/or missing chemistry in the model such as  
23 heterogeneous chemistry. Mao et al. (2013) suggest uptake of HO<sub>2</sub> to aerosols undergo  
24 reaction with transition metal ions to convert HO<sub>2</sub> to H<sub>2</sub>O, removing hydrogen oxides from  
25 the atmosphere. They show that this proposed mechanism decreases OH at the surface, as  
26 simulated by the GEOS-Chem model, and consequently increases CO mixing ratios by 20-30  
27 ppbv. While a 20-30 ppbv increase in CO over Thailand will not remove the high CO bias in  
28 our simulation, this heterogeneous chemistry may explain some of the underprediction of CO.  
29 When comparing the CO concentrations from the different WRF-chem simulations with the  
30 measurements in Thailand, we find the different WRF-chem results to be quite similar. An  
31 examination of the correlation coefficients (Table 3) reveals that these values are quite similar  
32 from simulation to simulation. This can be due in part to the fact that none of the emission

1 inventories are specific to the modeled time period. However, a paired difference test  
2 (Kruskal and Wallis, 1952) shows that there are statistical differences for CO among the  
3 different emission inventories at Khonkaen, Saraburi, Nonthaburi, and Chonburi for both  
4 March and December and for Chiang Mai for December. The variability in the biases of the  
5 modeled CO mixing ratios (Table 4) also suggests that the different emission inventories are  
6 causing the different CO mixing ratios between the model simulations. Because the  
7 simulation using RETRO emissions, especially for March has larger biases than the other  
8 simulations, the more recent CO emission inventories either better represent the emissions in  
9 general or are more similar to what the emissions were for 2008.

10 The modeled CO surface mixing ratios are compared to the MOPITT V6 gridded Level 3  
11 near-surface CO retrievals to evaluate the modeled spatial distribution (Figures 10 and 11).  
12 The MOPITT V6 data (Deeter et al. 2011; 2012; 2013; Worden et al. 2010), which we used in  
13 this paper, has improved near surface CO retrievals. This improvement is accomplished by  
14 using near-infrared and thermal-infrared observations simultaneously to enhance the retrieval  
15 sensitivity of CO in the lower troposphere. WRF-Chem is able to capture well the patterns of  
16 high CO over Southeast Asia and Southern China in March (Figure 10), but overpredicts CO  
17 over northern Thailand and Burma. These regions of high CO coincide with the location of  
18 biomass burning, indicating the FINN fire emissions are too high in this region. The  
19 predicted CO mixing ratios are similar in magnitude to MOPITT over the Malay and southern  
20 IndoChina peninsulas. For December when biomass burning is less important, the general  
21 spatial pattern of CO is represented by WRF-Chem for all the simulations (Figure 11). The  
22 modeled CO in December is generally higher than MOPITT, particularly in the regions of the  
23 highest mixing ratios in southern China and easternmost India.

### 24 **5.2.3 O<sub>3</sub> Evaluation**

25 Scatter plots of the 6-hourly daytime O<sub>3</sub> mixing ratios compared to the measurements at the  
26 six ground sites show that O<sub>3</sub> is generally overpredicted for each of the different emission  
27 inventories for both March and December (Figure 12) by up to 100 ppbv. Locations that  
28 showed good agreement for CO (e.g. Chiang Mai in March) have very poor agreement for O<sub>3</sub>.  
29 Despite the large scatter of model results for O<sub>3</sub> (Figure 12), the correlation coefficients are  
30 generally 0.5 and higher (Table 5) indicating that the model captures the O<sub>3</sub> trend well, but  
31 has a high bias. WRF-Chem O<sub>3</sub> biases (Table 6) range from -1 to 40 ppbv with MACCity and  
32 MACCity/SEAC4RS having the highest bias at Chiang Mai. In December (Figure 12), the

1 model-observation is generally better than in March, although WRF-Chem tends to  
2 overpredict O<sub>3</sub>, especially at Khonkaen and Saraburi in northeastern and central Thailand. In  
3 general, the comparison of the model results among the different emission inventories show  
4 fairly similar results for O<sub>3</sub> mixing ratios, correlation coefficients, and biases. The correlation  
5 coefficients among simulations mostly vary by <0.1, suggesting that the different  
6 anthropogenic emission inventories produce very little variation in modeled O<sub>3</sub>. A paired  
7 difference test (Kruskal and Wallis, 1952) of these surface O<sub>3</sub> mixing ratios shows that there  
8 are not any statistical differences for O<sub>3</sub> among the different emission inventories. Likewise,  
9 variation among the monthly-mean O<sub>3</sub> biases among the different simulations are < 15 ppbv  
10 and mostly < 7 ppbv. The higher O<sub>3</sub> bias in March compared to December, especially in  
11 Chiang Mai where there are large biomass burning sources (Amnuaylojaroen and Kreasuwun,  
12 2012), suggests that biomass burning emissions are more uncertain than anthropogenic  
13 emissions.

14 The O<sub>3</sub> vertical profiles resulting from the WRF-Chem simulations are compared to  
15 SHADOZ ozonesondes and MOZART4 model results at 3 locations, Hanoi, Vietnam,  
16 Watukosek-Java, Indonesia and Kuala Lumpur, Malaysia (Figure 13). Both Hanoi and  
17 Watukosek-Java are near the WRF-Chem model domain boundaries (Figure 5g). At  
18 Watukosek-Java in March, the WRF-Chem prediction is low below the 700 hPa level and too  
19 high above 600 hPa (Figure 13a), while the MOZART4 prediction is more similar to  
20 observations near the surface. In December, the WRF-Chem results agree well with the  
21 observations at Watukosek-Java from the surface to 300 hPa (Figure 13c). Above 300 hPa,  
22 the model overpredicts the O<sub>3</sub> mixing ratios until it reaches the stratosphere. At Kuala  
23 Lumpur, the WRF-Chem results have very good agreement with O<sub>3</sub> observations for March  
24 (Figure 13b), while the MOZART4 results are high compared to the observations below the  
25 600 hPa level. In December at Kuala Lumpur, the observations are higher than the model  
26 results in the free troposphere (Figure 13d). The free troposphere mixing ratios are likely  
27 from outside the domain where MOZART4 results are used as boundary conditions. The O<sub>3</sub>  
28 measurements from Hanoi, a subtropical location, show multiple layers of O<sub>3</sub> in the free  
29 troposphere with lowest O<sub>3</sub> values of 20 ppbv occurring at 200 hPa for the March time period  
30 (Figure 13e). The WRF-Chem and MOZART4 results are not able to replicate the layering  
31 structure, but the WRF-Chem results do have high O<sub>3</sub> values from 900 to 600 hPa, while  
32 MOZART4 O<sub>3</sub> remains below 60 ppbv throughout the troposphere. Neither model is able to  
33 predict the 20 ppbv minimum O<sub>3</sub> at 200 hPa. There is very little difference between the WRF-

1 Chem results from the simulations with different emission inventories for Hanoi and  
2 Watukosek-Java, except for near the surface at Watukosek-Java in March. At Kuala Lumpur,  
3 there is much more variation between model results with different emission inventories. O<sub>3</sub>  
4 from the SEAC4RS emissions inventory simulation is less than the O<sub>3</sub> from the other  
5 simulations and has the worst agreement with observations at Kuala Lumpur. This difference  
6 could be because the SEAC4RS emissions inventory lacks ship emissions. When the  
7 SEAC4RS emissions are combined with MACCity emissions, the O<sub>3</sub> mixing ratios are more  
8 similar to the other simulations.

#### 9 **5.2.4 NO<sub>2</sub> Evaluation**

10 The spatial distribution of the WRF-Chem and OMI tropospheric column NO<sub>2</sub> are shown in  
11 Figures 14 and 15 for March and December, respectively. In general, the WRF-Chem  
12 simulation is able to capture the NO<sub>2</sub> pattern well over land in March with high NO<sub>2</sub> columns  
13 over China, Burma, Vietnam, Laos and Thailand and low values over the southern and  
14 southeast region of the model domain. The WRF-Chem NO<sub>2</sub> column is generally less than the  
15 OMI NO<sub>2</sub> column. In March, the OMI NO<sub>2</sub> column values over land are  $>2 \times 10^{15}$  molecules  
16 cm<sup>-2</sup> with peak values of  $\sim 5 \times 10^{15}$  molecules cm<sup>-2</sup> over the Pearl River Delta, while WRF-  
17 Chem predicts  $1 \times 10^{15}$  molecules NO<sub>2</sub> cm<sup>-2</sup> or more. The WRF-chem peaks of  $\sim 5 \times 10^{15}$  occur  
18 in northern Thailand and Burma and not over the Pearl River Delta. On the other hand, the  
19 WRF-Chem model underpredicts NO<sub>2</sub> column in the southeastern region of the model  
20 domain. For March, the WRF-Chem NO<sub>2</sub> column mostly reflects the biomass burning  
21 emissions pattern (Figure 3), while for December WRF-Chem is more similar to the  
22 anthropogenic emissions (Figure 4). The OMI NO<sub>2</sub> column does not show the high NO<sub>2</sub> over  
23 northern Thailand and Burma where the model has high biomass burning emissions in March.  
24 To explain this difference, WRF-Chem fire emissions could be too high, or OMI may miss  
25 the high NO<sub>2</sub> because of clouds interfering with the instrument's view. In situ measurements  
26 would allow us to evaluate better the performance of the model.

27 The largest variation among the model simulations is in the region near Indonesia and is a  
28 result of both low NO<sub>2</sub> mixing ratios from the MOZART boundary conditions and different  
29 estimates for shipping emissions among the different inventories (Table 2, Figures 3 and 4).  
30 Both the RETRO ship emissions, which are 75-80% smaller than INTEX-B and MACCity  
31 ship emissions, and the SEAC4RS only simulation, which does not have ship emissions  
32 contribute to the variation. When the MACCity ship emissions are combined with the

1 SEAC4RS emissions (MACCity/SEAC4RS), the agreement with OMI NO<sub>2</sub> column is much  
2 better than the SEAC4RS only simulation. For example, the MACCity/SEAC4RS simulation  
3 agrees better with OMI NO<sub>2</sub> column than the SEAC4RS only simulation. The NO<sub>2</sub> column  
4 model-observation comparison for December (Figure 15) shows that WRF-Chem slightly  
5 underpredicts the NO<sub>2</sub> column, especially over the mainland. All five simulations predict  
6 relatively low NO<sub>2</sub> column over Burma with values of  $\sim 1 \times 10^{14}$  molecules cm<sup>-2</sup> while OMI  
7 NO<sub>2</sub> column reports values of 5-10 $\times 10^{14}$  molecules cm<sup>-2</sup>. Figure 4 shows that NO emissions  
8 in Burma are lower than the surrounding regions. The comparison to satellite data suggests  
9 that perhaps these emissions are too low.

## 10 **6 Discussion**

11 There are several aspects of the simulations that contribute to the underprediction of CO at the  
12 surface and the overprediction of O<sub>3</sub> at the surface. One is that the model simulation is for  
13 2008 while the emission inventories are appropriate for other years (RETRO for 2000,  
14 INTEX-B for 2006, MACCity for 2010, and SEAC4RS for 2012). While the grid spacing of  
15 36 km is better than global chemistry transport models, it is likely that small-scale features,  
16 e.g. urban regions and orography are not adequately represented in this simulation. For  
17 example, Chiang Mai is in a mountain valley where pollutants can easily accumulate. Another  
18 possible error could arise from the fire emissions. One issue with coarse resolution modeling  
19 of biomass burning emissions is that multiple fires in one model grid cell are aggregated into  
20 a single, bigger fire area. This aggregated information is used by the plumerise model in  
21 WRF-Chem, which may erroneously apply too much thermal buoyancy associated with the  
22 fires, resulting in emissions placed too high above the ground. For example, WRF-Chem  
23 results without the plumerise feature of biomass burning emissions, as illustrated by the  
24 March monthly-averaged CO vertical profiles at Yangon, Burma (Figure 16), show that  
25 injection into the lowest model level gives vertical profiles more consistent with MOZART  
26 results, which injects fire emissions into the lowest model level. Thus, in the simulations with  
27 the plumerise feature, O<sub>3</sub> precursor species (NMVOCs and NO<sub>x</sub>) may be placed in an  
28 environment where O<sub>3</sub> production is more productive than if the precursors were placed near  
29 the surface. While these results indicate a substantial difference in CO mixing ratios in the  
30 lowest 500 hPa of the atmosphere, observations of CO vertical profiles are needed to help  
31 evaluate the model predictions. In addition, trash burning emissions are not included in this  
32 study, yet have been shown to have a significant contribution to the air quality (Hodzic et al.,

1 2012). In reality, Southeast Asia has complex emission sources that not only include biomass  
2 burning and anthropogenic activities, but also biofuel and trash burning. To improve  
3 simulations of CO in the future, these other emissions should be included.

4 Another possible cause of the CO underprediction and O<sub>3</sub> overprediction at the surface is that  
5 the anthropogenic emissions are too low. Global estimates of CO sources (Kopacz et al. 2010)  
6 based on satellite, aircraft, and surface observations suggest that CO emissions over Southeast  
7 Asia are underestimated by nearly a factor of two. For the INTEX-B emissions, Zhang et al.  
8 (2009) reported an uncertainty of 185% and 37% for CO and NO emissions, respectively. We  
9 conducted sensitivity simulations with higher CO emissions by a factor of 2 and higher NO  
10 emissions by 40%. Additional sensitivity simulations were performed with only CO emissions  
11 greater by a factor of 2 (NO emissions remained the same as the original inventory). The  
12 sensitivity simulations were performed for March when biomass burning is a major  
13 contribution to the results. The results were compared to the six ground sites shown in Fig.  
14 5g. The higher emissions improve agreement for both O<sub>3</sub> and CO concentrations at the 6  
15 monitoring sites. For example, the O<sub>3</sub> prediction from the increased emission simulations, on  
16 average, improved the correlation term by ~18% and reduced the bias from 24 ppbv to 8  
17 ppbv. The high emissions simulations decreased, on average, the correlation for CO surface  
18 mixing ratios by 23-34%, but reduced the average bias from 250-264 ppbv to 184-224 ppbv.  
19 Interestingly, the high emissions simulations produced too much CO at Chiang Mai (CM) by  
20 over 400 ppbv, yet the O<sub>3</sub> bias at CM was reduced to 2-4 ppbv (from 38-40 ppbv). This  
21 suggests that either the CO emissions from biomass burning are too high, or co-emitted VOCs  
22 should have higher emissions. The SRB site, downwind of Bangkok, went from too little CO  
23 (bias = -150 ppbv for INTEX-B) to too much CO (bias = 173 ppbv for INTEX-B high  
24 emissions simulations) with only a 2 ppbv decrease in bias of O<sub>3</sub>. CO at SRT changed very  
25 little, because SRT is located away from urban and biomass-burning regions. At the same  
26 time, KK, NTB and CBR all have a better correspondence to observations as shown by the  
27 decreased bias. However, WRF-Chem still underpredicts CO at these sites. The higher  
28 emissions slightly improved the prediction of NO<sub>2</sub> mixing ratios increasing the correlation  
29 coefficient by 18% but not changing the bias on average. By comparing the simulation with  
30 increased CO and NO emissions to the simulation with only increase CO emissions, the  
31 results for O<sub>3</sub> and CO are very similar indicating that increased CO emissions caused the  
32 decrease in O<sub>3</sub> concentrations.

1 Our WRF-Chem simulations did not include heterogeneous chemistry, which can affect OH  
2 concentrations (Mao et al. 2013) and therefore CO oxidation. Kumar et al. (2014) also found  
3 decreased OH and O<sub>3</sub> mixing ratios when heterogeneous chemistry was included for a  
4 simulation of a dust event over India. For this high dust-loading example of the effect of  
5 heterogeneous chemistry, O<sub>3</sub> decreased by 10-20 ppbv.

6 The underprediction of NO<sub>2</sub> in all the WRF-chem simulations suggests that the anthropogenic  
7 NO<sub>x</sub> emissions are underestimated over the Southeast Asia. These errors in anthropogenic  
8 emission estimates are likely due to uncertainties in including all the CO or NO<sub>x</sub> sources from  
9 the different emission sectors and estimating the emission factors from the different sources.  
10 The variation in NO shipping emissions, as seen by the comparison of the simulation using  
11 only the SEAC4RS emissions without shipping emissions with the simulation using  
12 MACCity-SEAC4RS emissions, does produce substantial variation among model predictions  
13 of NO<sub>2</sub> (Figure 14) and O<sub>3</sub> (Figure 13). Therefore, it is important to include the shipping  
14 sector as part of the emissions inventory.

15 This paper did not include the REAS emissions inventory. For Southeast Asia the REAS v2.1  
16 CO emissions are similar to the TRACE-P (Streets et al., 2003) and INTEX-B (Zhang et al.,  
17 2009) emission inventories for years 2000 and 2006, respectively. The REAS v2.1 NO<sub>x</sub>  
18 emissions are also similar to the TRACE-P emissions inventory for 2000, but are lower than  
19 the INTEX-B inventory for year 2006 (Kurakawa et al., 2013). We would then expect the  
20 REAS v2.1 inventory to produce similar results for CO surface mixing ratios as the INTEX-B  
21 emissions inventory did, but have lower NO<sub>x</sub> mixing ratios, if the year 2006 REAS inventory  
22 is used. The 2008 REAS v2.1 emissions are 10-20% greater than their 2006 emissions. These  
23 increased emissions would likely give results for CO and O<sub>3</sub> surface mixing ratios that are  
24 <10% greater than the mixing ratios simulated in this study. To confirm this, additional WRF-  
25 Chem simulations should be done with the REAS emissions inventory.

26 The goal of this paper is to examine the differences in predicted CO and O<sub>3</sub> mixing ratios at  
27 the surface when different anthropogenic emission inventories are used. Table 6 lists  
28 monthly-average O<sub>3</sub> and CO mixing ratios on land for March and December for all of  
29 simulation cases. During the biomass-burning season (March), the average CO differs by less  
30 than 5 ppbv (<1% difference) among the different emission inventories, while average O<sub>3</sub>  
31 ranges from 146 to 160 ppbv (9% difference) among the different emission inventories. In  
32 December when anthropogenic emissions are greater than biomass burning emissions, the

1 differences in average CO and O<sub>3</sub> among the different emission inventories is very small (2  
2 ppbv for CO and 7 ppbv for O<sub>3</sub>). These small variations, which are also seen in the mean bias  
3 calculations for the ground-based sites (Tables 3 and 5), suggest that the choice of the  
4 emission inventory does not have a substantial effect on CO and O<sub>3</sub> surface concentrations,  
5 despite the different emission inventories having a ~30% variation for CO and 10% variation  
6 for NO emissions.

7 By comparing the March average mixing ratios to the December average mixing ratios (Table  
8 6), the importance of biomass burning emissions on O<sub>3</sub> and CO variability is revealed. In  
9 March, CO is 16% greater than CO in December for all simulations except that with RETRO  
10 emissions. The average O<sub>3</sub> in March is ~30% greater than average O<sub>3</sub> in December. These  
11 differences are much greater than those induced by the anthropogenic emissions in Southeast  
12 Asia. Thus, biomass burning emissions produce more variability in WRF-Chem simulation  
13 results than the different anthropogenic emission inventories.

## 14 **7 Conclusion**

15 This study presents WRF-Chem results to show the variability of emissions on surface O<sub>3</sub> and  
16 CO mixing ratios in Southeast Asia. The predicted meteorological fields are evaluated with  
17 reanalysis output (MERRA), satellite data (TRMM) and ground-based observations (GPCC)  
18 for 2-m temperature, wind, and precipitation. Surface CO and O<sub>3</sub> mixing ratios are compared  
19 to ground-based monitoring observations in Thailand. Surface CO is also compared to  
20 MOPITT satellite data. O<sub>3</sub> vertical profiles are compared with SHADOZ ozonesonde data,  
21 and the NO<sub>2</sub> tropospheric column is evaluated with OMI satellite data.

22 In general, the temperature and winds showed good agreement with MERRA output, although  
23 there was a slight underestimate of temperature and slight overestimate of wind speed.  
24 Precipitation was reasonably predicted for regions north of 10°N in comparison to TRMM  
25 and GPCC data, but was overestimated near the equator. By using a grid spacing of 36 km,  
26 the precipitation was generated mostly by the cumulus parameterization in the model resulting  
27 in a less reliable prediction of rain and convective mass fluxes between the boundary layer  
28 and mid- to upper troposphere. Surface O<sub>3</sub> mixing ratios were generally higher than  
29 observations and surface CO mixing ratios were lower than observations. Although the  
30 emission inventories were for years other than that simulated here, the differences in surface  
31 O<sub>3</sub> and CO mixing ratios among the simulations with different inventories were small. Thus,  
32 the model biases are likely not the result of the emission inventory trends used here, but more



1 likely caused by the omission of sources such as trash burning and biofuel use and  
2 uncertainties not fully captured in the current emission inventories. Sensitivity simulations  
3 with doubled CO emissions showed that the model-observation agreement improved  
4 substantially for CO and O<sub>3</sub>. Thus, further study of the role of different emission sectors on  
5 CO and O<sub>3</sub> can help elucidate where the major weaknesses are in the emission inventories. In  
6 addition, analysis of the contribution of CO, NO<sub>x</sub>, O<sub>3</sub>, and VOCs from outside the Southeast  
7 Asia region on the region's air quality should be compared with the contribution of the local  
8 emissions.

9 Simulations using different anthropogenic emissions created only a slight variability of O<sub>3</sub>  
10 and CO mixing ratios, while biomass burning emissions added more variability. The different  
11 anthropogenic emissions have up to 30% difference in CO emissions but only a small change  
12 of O<sub>3</sub> and CO mixing ratios of ~4.5% and ~8%, respectively, among the simulations. A  
13 statistical analysis showed that the different model results are statistically different for CO  
14 mixing ratios at the Thai monitoring sites, and none are statistically different for O<sub>3</sub> except in  
15 southern Thailand during March. By comparing March (when biomass burning is at its peak)  
16 surface mixing ratios to December values, it is found that biomass burning emissions  
17 substantially increase both O<sub>3</sub> and CO mixing ratios by ~30% and ~16%.

18 Southeast Asia is a region with complex terrain and emission sources at small scales. Thus,  
19 one important test to improve the regional-scale simulations of air quality in Southeast Asia  
20 would be to use model grid spacing of the order of 10 km or less. A higher grid resolution  
21 should also reduce errors in the injection height of biomass burning emissions. However, a  
22 high-resolution simulation needs emission inventories at equally high resolution. Inclusion of  
23 other types of emissions, e.g. trash emissions, in the current inventories could also improve  
24 the representation of the atmospheric chemistry in Southeast Asia. Lastly, particulate matter  
25 (aerosols) was not addressed in this study. Not only should their contribution to air quality be  
26 evaluated, but their impact on gas-phase photochemistry should be addressed.

27

## 28 **Acknowledgements**

29 The authors would like to thank the National Center for Atmospheric Research (NCAR)  
30 Advanced Study Program (ASP) for the scholarship to visit the Atmospheric Chemistry  
31 Division (ACD), the Center for Environmental Health, Toxicology and Management of  
32 Chemical, Chiang Mai University, Faculty of Science, Chiang Mai, Thailand for Ph.D.

1 scholarship, and the Graduate School Chiang Mai University for partially support. The study  
2 was partially supported by NSF CHEM award 1049058. We are thankful for the Thai  
3 Pollution Control Department (PCD) providing their O<sub>3</sub> and CO observation data. We also  
4 acknowledge the Global Modeling and Assimilation Office (GMAO) and the GES DISC for  
5 the dissemination of MERRA, the NASA Goddard Space Flight Center for providing  
6 SHADOZ data, and the NASA Langley Research Center Atmospheric Science Data Center  
7 for providing MOPITT data. Analyses and visualizations used in this paper were produced  
8 with the Giovanni online data system, developed and maintained by the NASA GES DISC.  
9 We acknowledge Gabriele Pfister and Sachin Ghude for their assistance with WRF-Chem  
10 simulations. The comments from Christine Wiedinmyer and Rajesh Kumar are greatly  
11 appreciated. NCAR is operated by the University Corporation for Atmospheric Research  
12 (UCAR) under sponsorship of the National Science Foundation.

13

## 1 **References**

- 2 Adhikary, B., Carmichael, G. R., Tang, Y., Leung, L. R., Qian, Y., Schauer, J. J., Stone, E.  
3 A., Ramanathan, V., and Ramana, M. V.: Characterization of South Asian Aerosols during  
4 the ABC-Post Monsoon Experiment (ABC-APMEX): A Regional-Scale Modeling  
5 Analysis, *J. Geophys. Res.*, 112, D22S22, doi:10.1029/2006JD008143, 2007.
- 6 Akimoto, H. and Narita, H.: Distribution of SO<sub>2</sub>, NO<sub>x</sub>, and CO<sub>2</sub> emissions from fuel  
7 combustion and industrial activities in Asia with 1°×1° resolution, *Atmos. Environ.*, 28,  
8 213–225, 1994.
- 9 Amnuaylojaroen, T. and Kreasuwun, J.: Investigation of Fine and Coarse Particulate Matter  
10 from Burning Areas in Chiang Mai, Thailand using the WRF/CALPUFF, *Chiang Mai J.*  
11 *Sci.*, 39(2), 1-16, 2012.
- 12 Boersma, K. F., Jacob, D. J., Eskes, H. J., Pinder, R. W., Wand, J., and Vander A, R. J.:  
13 Intercomparison of SCIAMACHY and OMI tropospheric NO<sub>2</sub> columns: Observing the  
14 diurnal evolution of chemistry and emissions from space, *J. Geophys. Res.*, 113, D16S26,  
15 doi:10.1029/2007JD008816, 2008.
- 16 Boersma, K. F., Jacob, D. J., Trainic, M., Rudich, Y., DeSmedt, I., Dirksen, R., and Eskes, H.  
17 J.: Validation of urban NO<sub>2</sub> concentrations and their diurnal and seasonal variations  
18 observed from the SCIAMACHY and OMI sensors using in situ surface measurements in  
19 Israeli cities, *Atmos. Chem. Phys.*, 9, 3867–3879, doi:10.5194/acp-9-3867-2009, 2009.
- 20 Bucsela, E. J., Celarier, E. A., Wening, M. O., Gleason, J. F., Veefkind, J. P., Boersma, K. F.,  
21 and Brinksma, E. J.: Algorithm for NO<sub>2</sub> vertical column retrieval from the Ozone  
22 Monitoring Instrument, *IEEE Trans. Geosci. Remote. Sens.*, 44, 1245–1258, 2006.
- 23 Chen, F. and Dudhia, J.: Coupling an advanced land-surface/hydrology model with the Penn  
24 State/ NCAR MM5 modeling system. Part I: Model description and implementation, *Mon.*  
25 *Weather. Rev.*, 129, 569-585, 2001.
- 26 Chin, M., Rood, R. B., Lin, S. -J., Muller, J. F., and Thompson, A. M.: Atmospheric sulfur  
27 cycle in the global model GOCART: Model description and global properties, *J. Geophys.*  
28 *Res.*, 105, 24671-24687, 2000.
- 29 Chou, M. -D. and Suarez, M. J.: An efficient thermal infrared radiation parameterization for  
30 use in general circulation models. NASA Tech. Memo. 104606, 3, 85 pp., NASA/GSFC,  
31 Greenbelt, MD, 1994.

- 1 Deeter, M. N.: MOPITT (Measurement of Pollution in the Troposphere) Version6 Product  
2 User's Guide, available at  
3 [http://www2.acd.ucar.edu/sites/default/files/mopitt/v6\\_users\\_guide\\_201309.pdf](http://www2.acd.ucar.edu/sites/default/files/mopitt/v6_users_guide_201309.pdf), (last  
4 access: 12 September 2014), 2013
- 5 Deeter, M. N., Worden, H. M., Gille, J. C., Edwards, D. P., Mao, D., and Drummond, J. R.:  
6 MOPITT multispectral CO retrievals: Origins and effects of geophysical radiance errors,  
7 *J. Geophys. Res.*, 116, D15303, doi: 10.1029/2011JD015703, 2011.
- 8 Deeter, M. N., Worden, H. M., Edwards, D. P., Gille, J. C., and Andrews, A. E.: Evaluation of  
9 MOPITT retrievals of lower-tropospheric carbon monoxide over the United States, *J.*  
10 *Geophys. Res.*, 117, D13306, doi:10.1029/2012JD017553, 2012.
- 11 Deeter, M. N., Martinez-Alonso, S., Edwards, D. P., Emmons, L. K., Gille, J. C., Worden, H.  
12 M., Pittman, J. V., Daube, B. C., and Wofsy, S. C.: Validation of MOPITT Version 5  
13 Thermal-infrared, near-infrared, and multispectral carbon monoxide profile retrievals for  
14 2000-2011, *J. Geophys. Res.*, 118, 6710–6725, doi:10.1002/jgrd.50272, 2013.
- 15 Deng, X., Tie, X., and Zhou, X.: Effects of Southeast Asia biomass burning on aerosols and  
16 ozone concentrations over the Pearl River Delta (PRD) region, *Atmos. Environ.*, 42, 8493-  
17 8501, doi: 10.1016/j.atmosenv.2008.08.013, 2008.
- 18 Emmons, L. K., Deeter, M. N., Gille, J. C., Edwards, D. P., Attie, J.-L., Warner, J., Ziskin, D.,  
19 Francis, G., Khattatov, B., Yudin, V., Lamarque, J. -F., Ho, S. -P., Mao, D., Chen, J. S.,  
20 Drummond, J., Novelli, P., Sachse, G., Coffey, M., Hannigan, J. W., Gerbig, C.,  
21 Kawakami, S., Kondo, Y., Takegawa, N., Schlager, H., Baehr, J., and Ziereis,  
22 H.: Validation of Measurements of Pollution in the Troposphere (MOPITT) CO retrievals  
23 with aircraft in situ profiles, *J. Geophys. Res.*, 109, D03309, doi:10.1029/2003JD004101,  
24 2004.
- 25 Emmons, L. K., Pfister, G. G., Edwards, D. P., Gille, J. C., Sachse, G., Blake, D., Wofsy, S.,  
26 Gerbig, C., Matross, D., and Nedelec, P.: Measurements of Pollution in the Troposphere  
27 (MOPITT) validation exercises during summer 2004 field campaigns over North America,  
28 *J. Geophys. Res.*, 112, D12S02, doi:10.1029/2006JD007833, 2007.
- 29 Emmons, L. K., Edwards, D. P., Deeter, M. N., Gille, J. C., Campos, T., Nedelec, P., Novelli,  
30 P., and Sachse, G.: Measurements of Pollution In The Troposphere (MOPITT) validation  
31 through 2006, *Atmos. Chem. Phys.*, 9, 1795-1803, 2009.
- 32 Emmons, L. K., Walters, S., Hess, P. G., Lamarque, J. -F., Pfister, G. G., Fillmore, D.,

1 Granier, C., Guenther, A., Kinnison, D., Laepple, t., Orlando, J., Tie, X., Tyndall, G.,  
2 Wiedinmyer, C., Baughcum, S. L., and Kloser, S.: Description and evaluation of the Model  
3 for Ozone and Related chemical Tracers, version 4 (MOZART4), *Geosci. Model. Dev.*, 3,  
4 43-67, 2010.

5 Fast, J. D., Gustafson Jr, W. I., Easter, R. C., Zaveri, R. A., Barnard, J. C., Chapman, E. G.,  
6 and Grell, G. A.: Evolution of ozone, particulates, and aerosol direct forcing in an urban  
7 area using a new fully-coupled meteorology, chemistry, and aerosol model, *J. Geophys.*  
8 *Res.*, 111:D21305, doi:10.1029/2005JD006721, 2006.

9 Geng, F., Tie, X., Guenther, A., Li, G., Cao, J., and Harley, P.: Effect of isoprene emissions  
10 from major forests on ozone formation in the city of Shanghai, China, *Atmos. Chem.*  
11 *Phys.*, 11, 10449-10459, doi:10.5194/acp-11-10449-2011, 2011

12 Ghude, S. D., Pfister, G. G., Jena, C. K., Van der A, R. J., Emmons, L. K. and Kumar, R.:  
13 Satellite constraints of Nitrogen Oxide (NO<sub>x</sub>) emissions from India based on OMI  
14 observations and WRF-Chem simulations, *Geophys. Res. Lett.*,  
15 doi:10.1029/2012GL053926, 2013.

16 Granier, C., Bessagnet, B., Bond, T., Angiola, A. D., Van Der Gon, H. D., Frost, G. J., Heil,  
17 A., Kaiser, J. W., Kinne, S., Klimont, Z., Kloster, S., Lamarque, J. -F., Liousse, C., Masui,  
18 T., Meleux, F., Mieville, A., Ohara, T., Raut, J.-C., Riahi, K., Schultz, M. G., Smith, S. J.,  
19 Thompson, A., Aardenne, J. V., Vander Werf, G. R., and Van Vuuren, D. P.: Evolution of  
20 anthropogenic and biomass burning emission of air pollutants at global and regional scales  
21 during the 1980-2010 period, *Climatic Change*, 109, 163-190, 2011.

22 Grell, G. A. and Devenyi, D.: A generalized approach to parameterizing convection  
23 combining ensemble and data assimilation techniques, *Geophys. Res. Lett.*, 29,  
24 doi:10.1029/2002GL015311, 2002.

25 Grell, G. A., Peckham, S. E., Schmitz, R., McKeen, S. A., Frost, G., Skamarock, W. C., and  
26 Eder, B.: Fully coupled "online" chemistry within the WRF model, *Atmos. Environ.*, 29,  
27 6957-6975, 2005.

28 Guenther, A., Karl, T., Harley, P., Wiedinmyer, C., Palmer, P., and Geron, C.: Estimates of  
29 global terrestrial isoprene emissions using MEGAN (Model of Emissions of Gases and  
30 Aerosols from Nature), *Atmos. Chem. Phys.*, 6, 3181-3210, 2006.

31 Han, Z., Sakurai, T., Ueda, H., Matsuda, K., Hozumi, Y., Carmichael, G. R., Streets, D. G.,  
32 Park, S. U., Fung, C., Chang, A., Kajino, M., Thongboonchoo, N., Engardt, M., Bennet,  
33 C., Hayami, H., Sartelet, K., Holloway, T., Wang, Z., and Amann, M.: Model

1 Intercomparison and Evaluation of Ozone and Relevant Species – MICS-Asia Phase II  
2 Study, *Atmos. Environ.*, 42, 3491-3509, 2008

3 Hodzic, A., Wiedinmyer, C., Salcedo, D., and Jimenez, J. L.: Impact of trash burning on air  
4 quality in Mexico City, *Environ. Sci. Tech.*, 46, 4950-4957, doi: 10.1021/es203954r, 2012.

5 Hollingsworth, A., Engelen, R. J., Textor, C., Benedetti, A., Boucher, O., Chevallier, F.,  
6 Dethof, A., Elbern, H., Eskes, H., Flemming, J., Granier, C., Morcrette, J. J., Rayner, P.,  
7 Peuch, V. -H., Rouil, L., Schultz, M., and Simmons, A. J.: Toward a monitoring and  
8 forecasting system for atmospheric composition: the GEMS Project, *Bull. Amer. Meteor.  
9 Soc.*, 89, 1147–1164. doi:10.1175/2008BAMS2355.1, 2008.

10 Huffman, G. J. and Bolvin, D. T.: TRMM and Other Data Precipitation Data Set Document,  
11 available at [ftp://precip.gsfc.nasa.gov/pub/trmmdocs/3B42\\_3B43\\_doc.pdf](ftp://precip.gsfc.nasa.gov/pub/trmmdocs/3B42_3B43_doc.pdf) (last access: 14  
12 September 2014), 2012.

13 Huffman, G. J., Adler, R. F., Arkin, P., Chang, A., Ferraro, R., Gruber, A., Janowiak, J.,  
14 McNab, A., Rudolph, B., and Schneide, U.: The Global Precipitation Climatology Project  
15 (GPCP) combined precipitation dataset, *Bull. Amer. Meteor. Soc.*, 78, 5–20, 1997.

16 Janjic, Z. I.: Nonsingular Implementation of the Mellor–Yamada Level 2.5 Scheme in the  
17 NCEP Meso model, NCEP Office Note, No. 437, 61, 2002.

18 Koo, M.-S., and Hong, S.-Y.: Diurnal variations of simulated precipitation over East Asia in  
19 two regional climate models, *J. Geophys. Res.*, 115, D05105, doi:10.1029/2009JD012574.  
20 2010.

21 Kopacz, M., Jacob, D. J., Fisher, J. A., Logan, J. A., Zhang, L., Megretskaia, I. A., Yantosca,  
22 R. M., Singh, K., Henze, D. K., Burrows, J. P., Buchwitz, M., Khlystova, I., McMillan, W.  
23 W., Gille, J. C., Edward, D. P., Eldering A., Thouret, V., and Nedlec, P.: Global estimates  
24 of CO sources with high resolution by adjoint inversion of multiple satellite datasets  
25 (MOPITT, AIRS, SCIAMACHY, TES), *Atmos. Chem. Phys.*, 10, 855-876, 2010.

26 Kramer, L. J., Leigh, R. J., Remedios, J. J., and Monks, P. S.: Comparison of OMI and  
27 ground-based in situ and MAX-DOAS measurements of tropospheric nitrogen dioxide in  
28 an urban area, *J. Geophys. Res.*, 113, D16S39, doi:10.1029/2007jd009168, 2008.

29 Kruskal, W. H., and Wallis, W. A.: Use of ranks in one-criterion variance analysis, *J. Am.  
30 Statist. Assoc.*, 47, 583-621, doi:10.1080/01621459.1952.10483441, 1952.

31 Kumar, R., Naja, M., Pfister, G. G., Barth, M. C., and Brasseur, G. P.: Source attribution of  
32 carbon monoxide in India and surrounding regions during wintertime, *J. Geophys. Res.*,  
33 118, 1981-1995, DOI: 10.1002/jgrd.50134, 2013.

1 Kumar, R., Barth, M. C., Madronich, S., Naja, M., Carmichael, G. R., Pfister, G. G., Knote,  
2 C., Brasseur, G. P., Ojha, N., and Sarangi, T.: Effect of dust aerosols on tropospheric  
3 chemistry during a typical pre-monsoon season dust storm in northern India, *Atmos. Chem.*  
4 *Phys.*, 14, 6813-6834, 2014.

5 Kurokawa, J., Ohara, T., Morikawa, T., Hanayama, S., Janssens-Maenhout, G., Fukui, T.,  
6 Kawashima, K., and Akimoto, H.: Emissions of air pollutants and greenhouse gases over  
7 Asian regions during 2000-2008: Regional Emission inventory in ASia (REAS) version 2,  
8 *Atmos. Chem. Phys.*, 13, 11,019-11,058, 2013.

9 Lamarque, J. -F., Bond, T. C., Eyring, V., Granier, C., Heil, A., Klimont, Z., Lee, D., Liousse,  
10 C., Mieville, A., Owen, B., Schultz, M. G., Shindell, D., Smith, S. J., Stehfest, E., Van  
11 Aardenne, J., Cooper, O. R., Kainuma, M., Mahowald, N., McConnell, J. R., Naik, V.,  
12 Riahi, K., and van Vuuren, D. P.: Historical (1850–2000) gridded anthropogenic and  
13 biomass burning emissions of reactive gases and aerosols: methodology and application,  
14 *Atmos. Chem. Phys.*, 10, 7017-7039, 2010.

15 Liu, C. -H., Yeh, M. T., and Paul, S.: Effect of anthropogenic emissions in East Asia on  
16 regional ozone levels during spring cold continental outbreaks near Taiwan: A case study,  
17 *Environ. Modell. Softw.*, 23, 579-591, 2008.

18 Lu, Z. and Streets, D. G.: The Southeast Asia Composition, Cloud, Climate Coupling  
19 Regional Study Emission Inventory, <http://bio.cgrer.uiowa.edu/SEAC4RS/emission.html>  
20 (last access: 12 September 2014), 2012.

21 Mao, J., Fan, S., Jacob, D. J., and Travis, K. R.: Radical loss in the atmosphere from Cu-Fe  
22 redox coupling in aerosol, *Atmos. Chem. Phys.*, 13, 509-519, 2013.

23 Mlawer, E. J., Taubman, S. J., Brown, P. D., Iacono, M. J., and Clough, S.A.: Radiative  
24 transfer for inhomogeneous atmosphere: RRTM, a validated correlated-k model for the  
25 longwave, *J. Geophys. Res.*, 102, 16663–16682, 1997.

26 Neu, J. L. and Prather, M. J.: Toward a more physical representation of precipitation  
27 scavenging in global chemistry models: cloud overlap and ice physics and their impact on  
28 tropospheric ozone, *Atmos. Chem. Phys.*, 12, 3289-3310, 2012.

29 Ohara, T., Akimoto, H., Kurokawa, J., Horii, N., Yamaji, K., Yan, X., and Hayasaka, T.: An  
30 Asian emission inventory of anthropogenic emission sources for the period 1980–2020,  
31 *Atmos. Chem. Phys.*, 7, 4419–4444, 2007.

1 Olivier, J. G. J., Van Aardenne, J. A., Dentener, F., Ganzeveld, L., and Peters, J. A. H. W.:  
2 Recent trends in global greenhouse gas emissions: regional trends and spatial distribution  
3 of key sources, *Environ. Sci.*, 2, 81-99, doi: 10.1080/15693430500400345, 2005.

4 Rienecker, M. M., Suarez, M. J., Gelaro, R., Todling, R., Bacmeister, J., Liu, E., Bosilovich,  
5 M. G., Schubert, S. D., Takacs, L., Kim, G. -K., Bloom, S., Chen, J., Collins, D., Conaty,  
6 A., Da Silva, A., Gu, W., Joiner, J., Koster, R. D., Lucchesi, R., Molod, A., Owens, T.,  
7 Pawson, S., Pegion, P., Redder, C. R., Reichle, R., Robertson, F. R., Ruddick, A. G.,  
8 Sienkiewicz, M., and Woollen, J.: MERRA - NASA's Modern-Era Retrospective Analysis  
9 for Research and Applications, *J. Climate*, 24, 3624-3648, doi: 10.1175/JCLI-D-11-  
10 00015.1, 2011.

11 Rudolf, B. and Schneider, U.: Calculation of Gridded Precipitation Data for the Global Land-  
12 Surface using in-situ Gauge Observations, Proceedings of the 2nd Workshop of the  
13 International Precipitation Working Group IPWG, Monterey, 25-28 October 2004,  
14 EUMETSAT, 231-247, 2005.

15 Sandu, A. and Sander, R.: Technical note: Simulating chemical systems in Fortran90 and  
16 Matlab with the Kinetic PreProcessor KPP-2.1, *Atmos. Chem. Phys.*, 6, 187-195,  
17 doi:10.5194/acp-6-187-2006, 2006.

18 Schaap. M., Roemer, M., Sauter, F., Boersen, G., Timmermans, R., Builtjes, P.J.H.,  
19 Vermeulen, A.T., LOTOS-EUROS: Documentation, TNO-report: B&O-A R 2005/297,  
20 available at: <http://www.lotos-euros.nl/doc/LOTOS-EUROS-v11-documentation.pdf> (last  
21 access: 12 September 2014), 2005.

22 Schneider, U., Becker, A., Meyer-Christofer, A. Ziese, M., and Rudolf, B.: Global  
23 Precipitation Analysis Products of the GPCC, available at:  
24 [ftp://ftp.dwd.de/pub/data/gpcc/PDF/GPCC\\_intro\\_products\\_2008.pdf](ftp://ftp.dwd.de/pub/data/gpcc/PDF/GPCC_intro_products_2008.pdf) (last access: 12  
25 September 2014), 2011a.

26 Schneider, U., Becker, A., Finger, P., Meyer-Christoffer, A., Rudolf, B., Ziese, M.: GPCC  
27 Full Data Reanalysis Version 6.0 at 1.0deg: Monthly Land-Surface Precipitation from Rain  
28 Gauges built on GTS-based and Historic Data, doi:10.5676/DWD\_GPCC/FD\_M\_V6\_100,  
29 2011b.

30 Schultz, M., Rast, S., van het Bolscher, M., Pulles, T., Pereira, J., Spessa, A., Dalsøren, S.,  
31 van Noije, T., and Szopa, S.: REanalysis of the TROpospheric chemical composition over  
32 the past 40 years, A long-term global modeling study of tropospheric chemistry funded  
33 under the 5th EU framework programme. Tech. rep., EU-Contract No. EVK2-CT-2002-



1 00170, available at: [ftp://ftp.retro.enes.org/pub/documents/reports/D1-6\\_final.pdf](ftp://ftp.retro.enes.org/pub/documents/reports/D1-6_final.pdf) (last  
2 access: 12 September 2014), 2007.

3 Skamarock, W. C., Klemp, J. B., Duhia, J., Gill, D. O., Barker, D. M., Duda, M. G., Huang,  
4 X. -Y., Wang, W., and Powers, J. G.: A Description of the Advanced Research WRF  
5 Version 3, NCAR Technical note, National Center for Atmospheric Research, Boulder,  
6 CO, USA, 2008.

7 Shepard, D.: A two-dimensional interpolation function for irregularly spaced data. In  
8 Proceedings of the 1968 23rd ACM National Conference, ACM, New York, NY, 517-524,  
9 1968.

10 Stauffer, D. R. and Seaman, N. L.: Use of four-dimensional data assimilation in a limited area  
11 mesoscale model. Part I: Experiments with synoptic-scale data, *Mon. Weather. Rev.*, 118,  
12 1250–1277, 1990.

13 Streets, D. G., Bond, T. C., Carmichael, G. R., Fernandes, S. D., Fu, Q., He, D., Klimont, Z.,  
14 Nelson, S. M., Tsai, N. Y., Wang, M. Q., Woo, J. -H., and Yarber, K. F.: An inventory of  
15 gaseous and primary aerosol emissions in Asia in the year 2000, *J. Geophys. Res.*, 108,  
16 8809, doi:10.1029/2002JD003093, 2003.

17 Tanimoto, H., Ohara, T., and Uno, I.: Asian anthropogenic emissions and decadal trends in  
18 springtime tropospheric ozone over Japan: 1998-2007, *Geophys. Res. Lett.*, 36,  
19 doi:10.1029/2009GL041382, 2009

20 Thompson, A. M., Miller, S. K., Tilmes, S., Kollonige, D. W., Witte, J. C., Oltmans, S. J.,  
21 Johnson, B. J., Fujiwara, M., Schmidlin, F. J., Coetzee, G. J. R., Komala, N., Maata, M.,  
22 Mohamad, M., Nguyo, J., Mutai, C., Ogino, S. -Y., Da Silva, R. F., Paes Leme, N. M.,  
23 Posny, F., Scheele, R., Selkirk, H. B., Shiotani, M., Stubi, R., Levrat, G., Calpini, B.,  
24 Thouret, V., Tsuruta, H., Canossa, J. V., Vomel, H., Yonemura, S., Diaz, J. A., Tan Thanh,  
25 N. T., and Ha, T.: Southern Hemisphere Additional Ozonesondes (SHADOZ) ozone  
26 climatology (2005-2009): Tropospheric and tropical tropopause layer (TTL) profiles with  
27 comparisons to OMI-based ozone products, *J. Geophys. Res.*, 117, D23301,  
28 doi:10.1029/2011JD016911, 2012

29 Thompson, G., Rasmussen, R. M., and Manning, K.: Explicit forecasts of winter precipitation  
30 using an improved bulk microphysics scheme. Part I: Description and sensitivity analysis,  
31 *Mon. Weather. Rev.*, 132, 519–542, 2004.

1 Tie, X., Madronich, S., Walters, S., Zhang, R., Rasch, P., and Collins, W.: Effects of clouds  
2 on photolysis and oxidants in the troposphere, *J. Geophys. Res.*, 108(D20), doi:  
3 10.1029/2003JD003659, 2003.

4 Van Vuuren D. P., Edmonds, J., Kainuma, M., Riahi, K., Thomson, A., Hibbard, K., Hurtt, G.  
5 C., Kram, T., Krey, V., and Lamarque, J. –F.: The representative concentration pathways:  
6 an overview, *Climatic Change*, 109, 5-31, 2011.

7 Wang, H., Skamarock, W. C., and Feingold, G.: Evaluation of Scalar Advection Schemes in  
8 the Advanced Research WRF Model Using Large-Eddy Simulations of Aerosol-Cloud  
9 Interactions, *Mon. Weather. Rev.*, 137, 2547–2558, 2009.

10 Wang, X., Carmichael, G. R., Chen, D., Tang, Y., and Wang, T.: Impacts of different  
11 emission sources on air quality during March 2001 in the Pearl River Delta (PRD) region,  
12 *Atmos. Environ.*, 39, 5227-5241, 10.1016/j.atmosenv.2005.04.035, 2005.

13 Wang, Y., Zhang, Y., and Hao, J.: Seasonal and spatial variability of surface ozone over  
14 China: contribution from background and domestic pollution, *Atmos. Chem. Phys.*, 7,  
15 3511-3525, doi:10.5194/acp-11-3511-2011, 2011

16 Wesley, M. L.: Parameterization of surface resistance to gaseous dry deposition in regional  
17 numerical models, *Atmos. Environ.*, 16, 1293-1304, 1989.

18 Wiedinmyer, C., Akagi, S. K., Yokelson, R. J., Emmons L, K., Al-Saadi J. A., Orlando J. J.,  
19 and Soja A. J.: The Fire Inventory from NCAR (FINN): a high resolution global model to  
20 estimate the emissions from open burning, *Geosci. Model. Dev.*, 3, 2439-2476, 2010.

21 Willmott, C. J., Rowe, C. M., Philpot, W. D.: Small scale climate maps: a sensitivity analysis  
22 of some common assumption associated with grid point interpolation and contouring, *Am.*  
23 *Cartographer*, 12, 5-16, 1985.

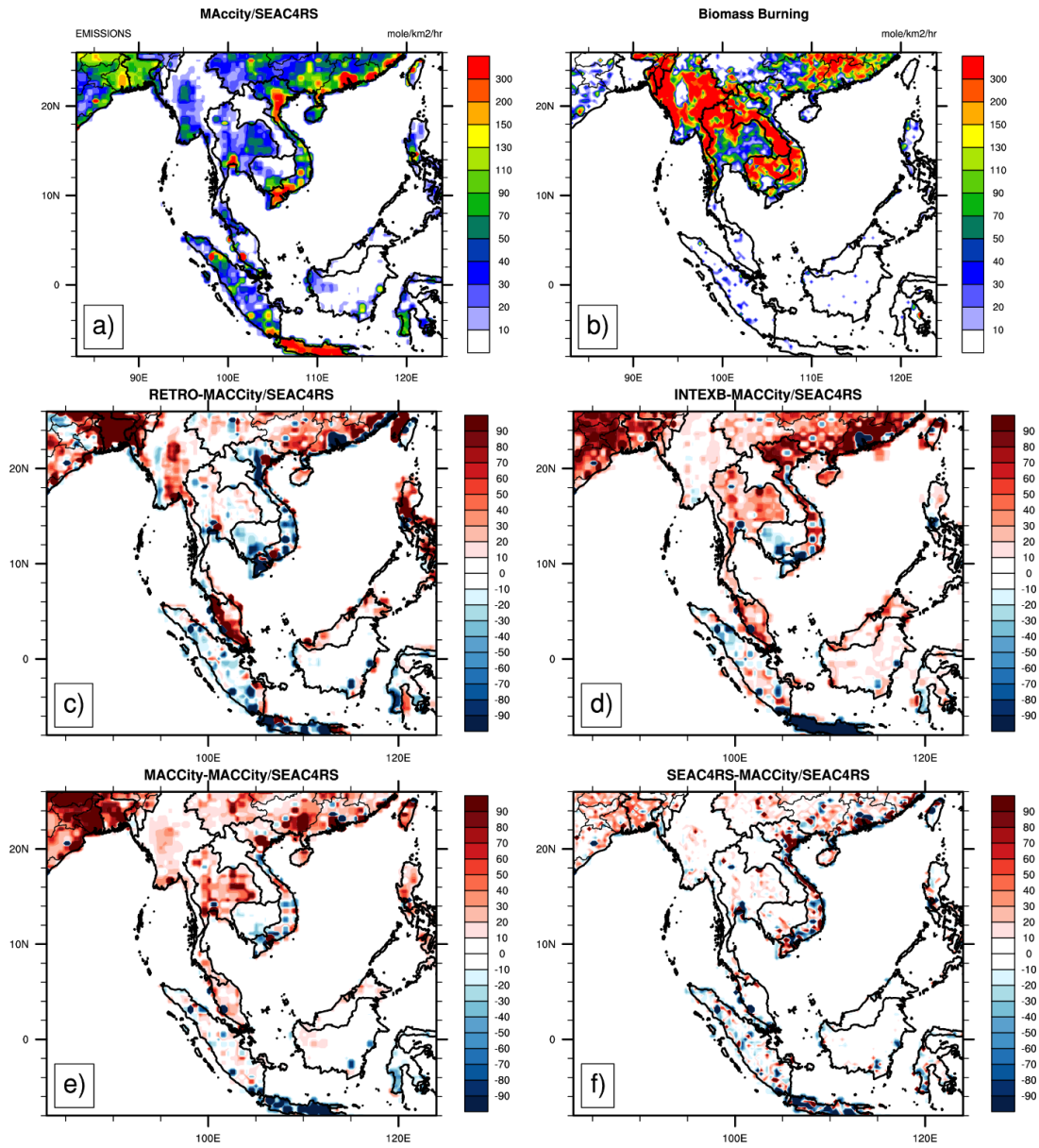
24 Worden, H. M., Deeter, M. N., Edwards, D. P., Gille, J. C., Drummond, J. R., and Nédélec,  
25 P.: Observations of near-surface carbon monoxide from space using MOPITT multispectral  
26 retrievals, *J. Geophys., Res.*, 115, D18314, doi:10.1029/2010JD014242, 2010.

27 Zhang, Q., Streets, D. G., Carmichael, G. R., He, K. B., Huo, H., Kannari, A., Klimont, Z.,  
28 Park, I. S., Reddy, S., Fu, J. S., Chen, D., Duan, L., Lei, Y., Wang, L. T., and Yao, Z. L.:  
29 Asian emissions in 2006 for the NASA INTEX-B mission, *Atmos. Chem. Phys.*, 9, 5131-  
30 5153, 2009.

31 Zhou, Y., Brunner, D., Boersma, K. F., Dirksen, R., and Wang, P.: An improved tropospheric  
32 NO<sub>2</sub> retrieval for OMI observations in the vicinity of mountainous terrain, *Atmos. Meas.*  
33 *Tech.*, 2, 401–416, doi:10.5194/amt-2-401-2009, 2009.

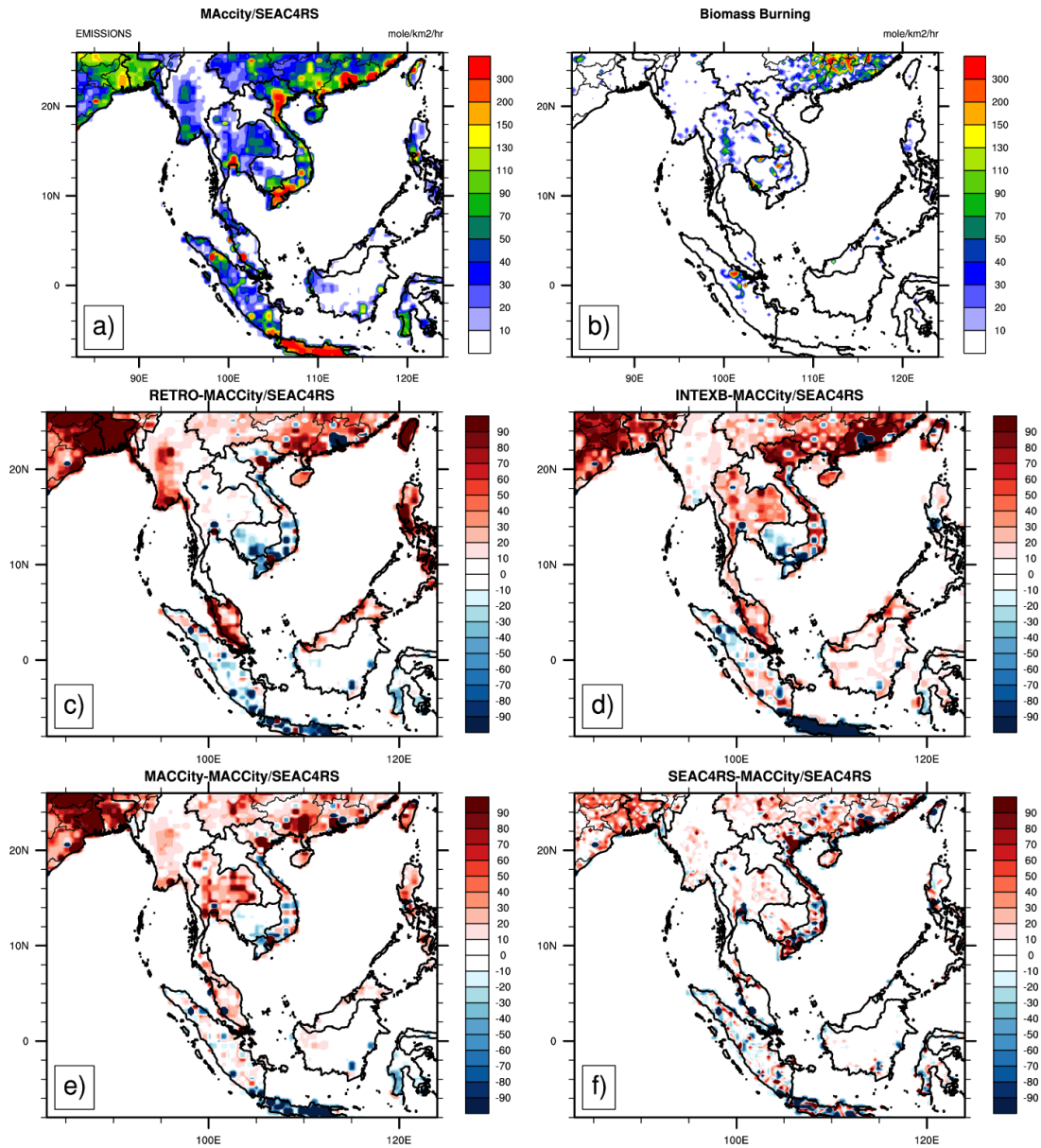
34

# E\_CO, (mole/km2/hr)



1  
2 Figure 1. CO emissions for March 2008 from different emission inventories a)  
3 MACCity/SEAC4RS, b) Biomass Burning, c) RETRO-MACCity/SEAC4RS, d) INTEXB-  
4 MACCity/SEAC4RS, e) MACCity-MACCity/SEAC4RS, and f) SEAC4RS-  
5 MACCity/SEAC4RS.

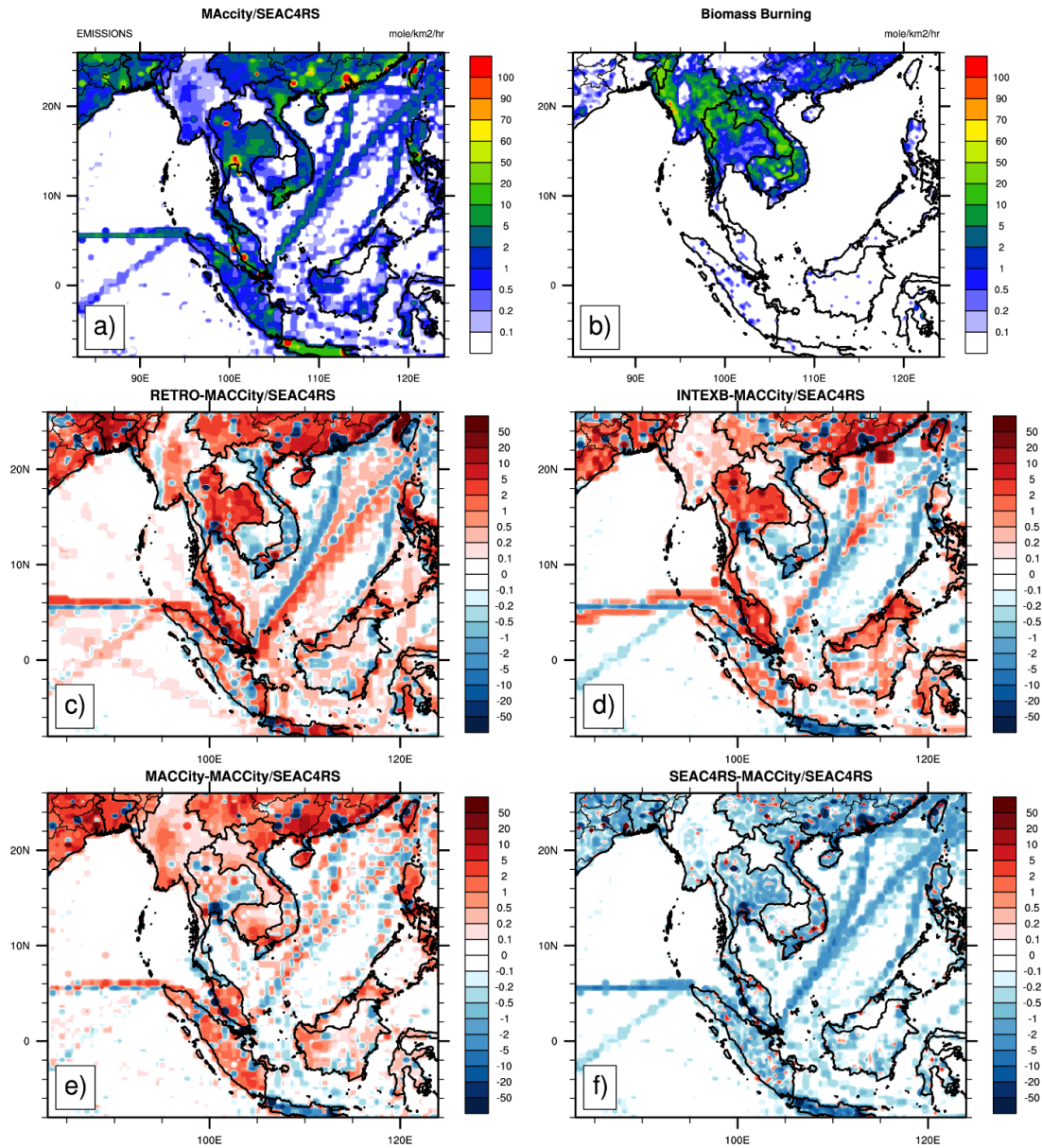
# E\_CO, (mole/km<sup>2</sup>/hr)



1

2 Figure 2. CO emissions for December 2008 from different emission inventories a)  
3 MACCity/SEAC4RS, b) Biomass Burning, c) RETRO-MACCcity/SEAC4RS, d) INTEXB-  
4 MACCity/SEAC4RS, e) MACCity-MACCcity/SEAC4RS, and f) SEAC4RS-  
5 MACCity/SEAC4RS.

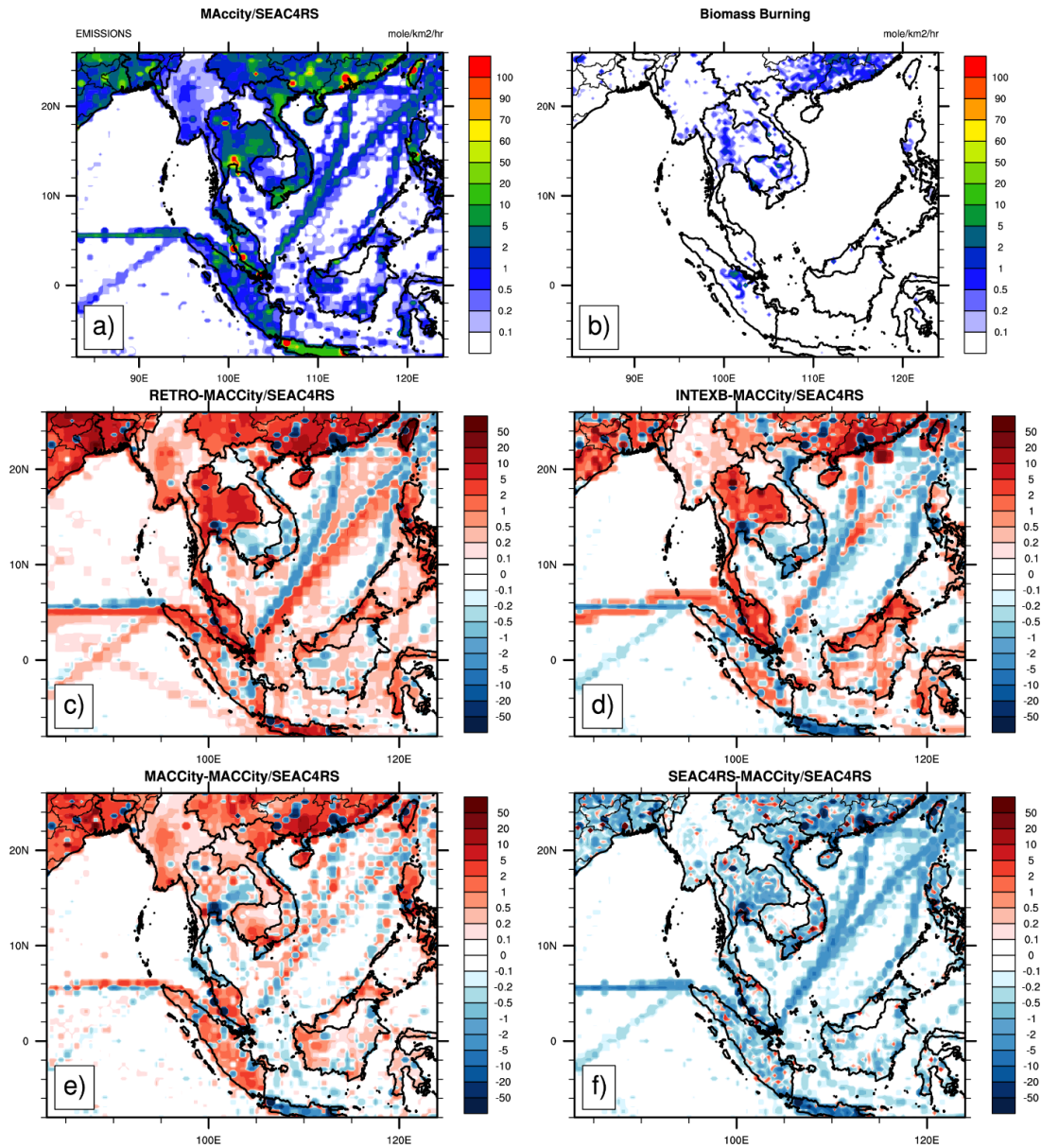
# E\_NO, (mole/km<sup>2</sup>/hr)



1

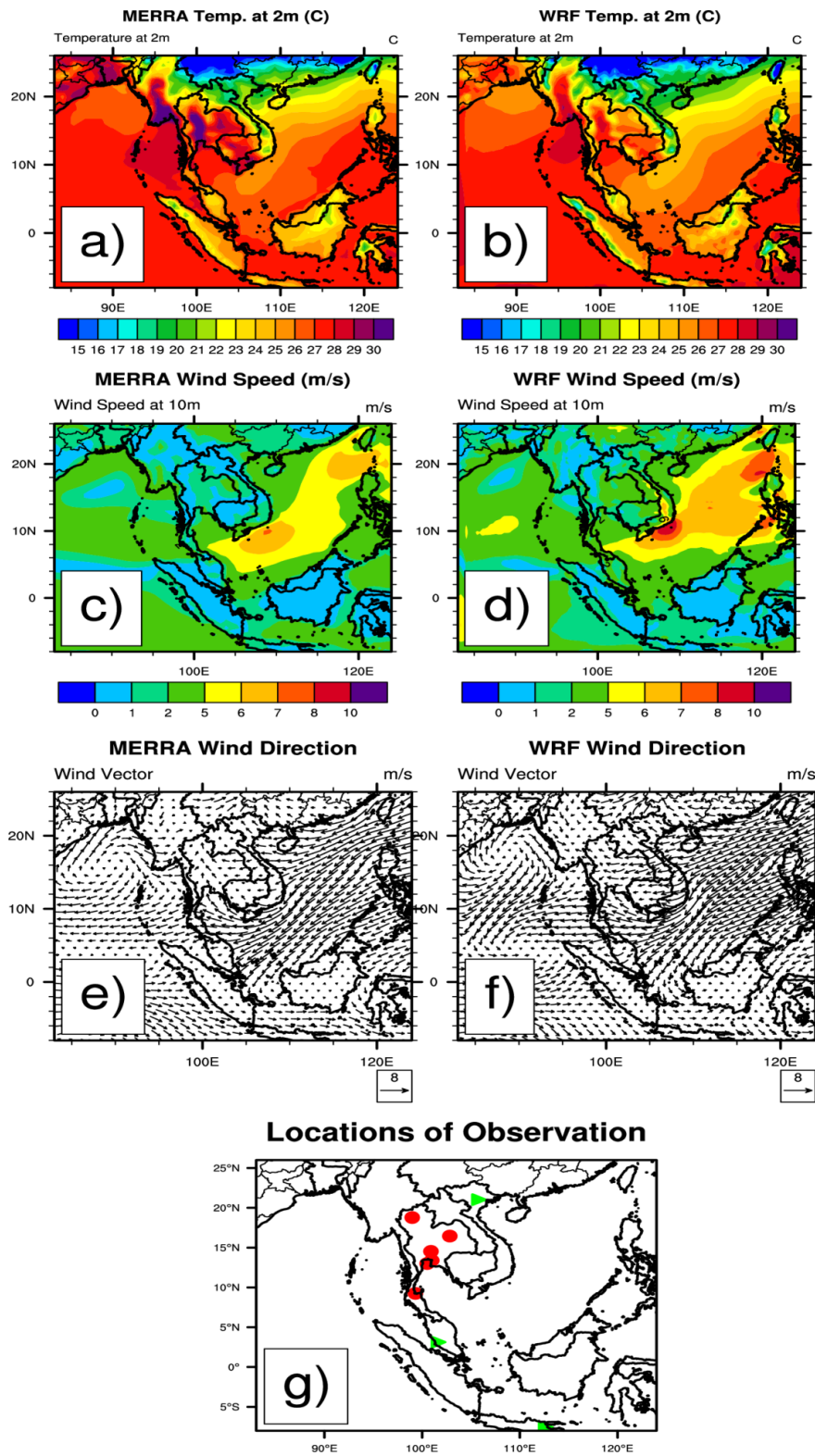
2 Figure 3. Nitrogen oxides emissions for March 2008 from different emission inventories a)  
3 MAccity/SEAC4RS, b) Biomass Burning, c) RETRO-MAccity/SEAC4RS, d) INTEXB-  
4 MAccity/SEAC4RS, e) MAccity-MAccity/SEAC4RS, and f) SEAC4RS-  
5 MAccity/SEAC4RS.

# E\_NO, (mole/km<sup>2</sup>/hr)



1

2 Figure 4. Nitrogen oxides emissions for December 2008 from different emission inventories  
3 a) MACCity/SEAC4RS, b) Biomass Burning, c) RETRO-MACCity/SEAC4RS, d) INTEXB-  
4 MACCity/SEAC4RS, e) MACCity-MACCity/SEAC4RS, and f) SEAC4RS-  
5 MACCity/SEAC4RS.

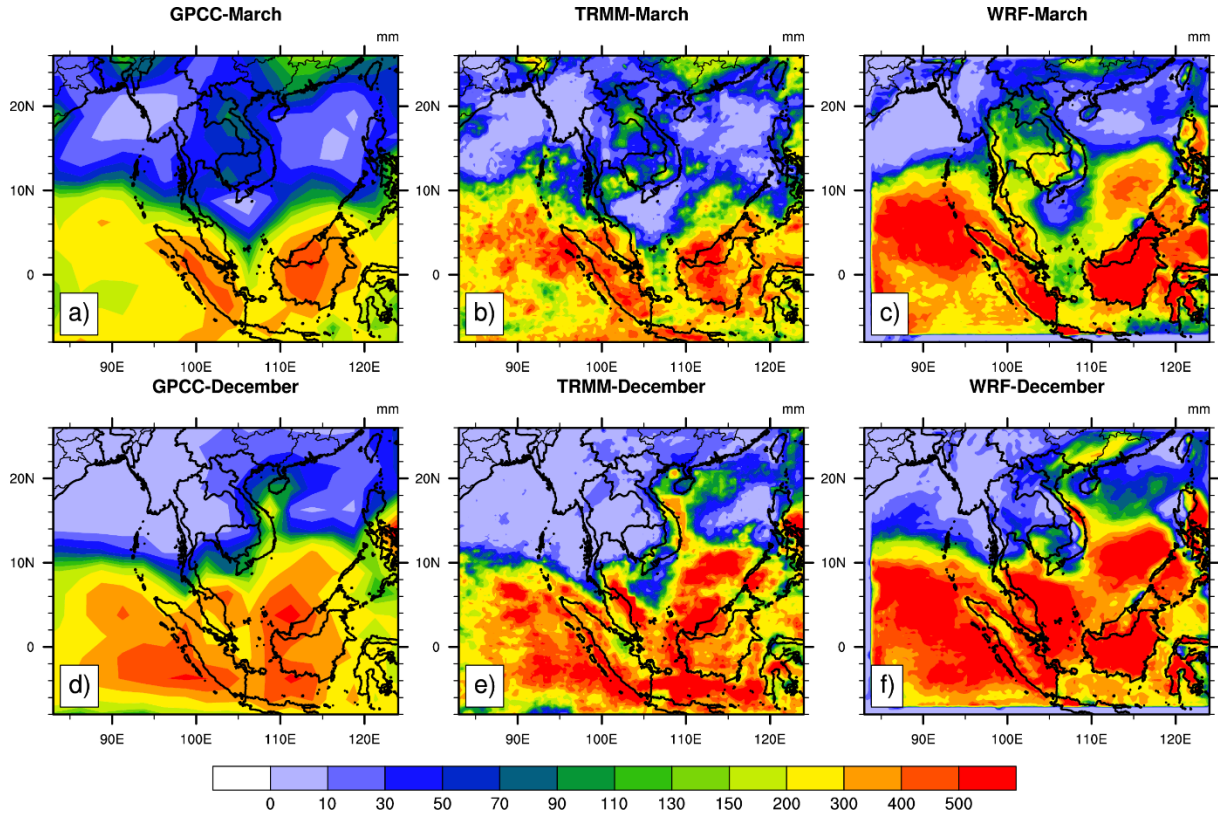


1  
 2 Figure 5. March 2008 monthly-averaged a) 2-m temperature ( $^{\circ}\text{C}$ ) from MERRA, b) 2-m  
 3 temperature ( $^{\circ}\text{C}$ ) from WRF, c) 10-m wind speed ( $\text{m s}^{-1}$ ) from MERRA, d) 10-m wind speed  
 4 ( $\text{m s}^{-1}$ ) from WRF, e) 10-m wind direction from MERRA, and f) 10-m wind direction from

1 WRF. g) Locations of ground-based CO and O<sub>3</sub> measurements (red dot) and ozonesonde sites  
2 (green triangle) are marked.

3

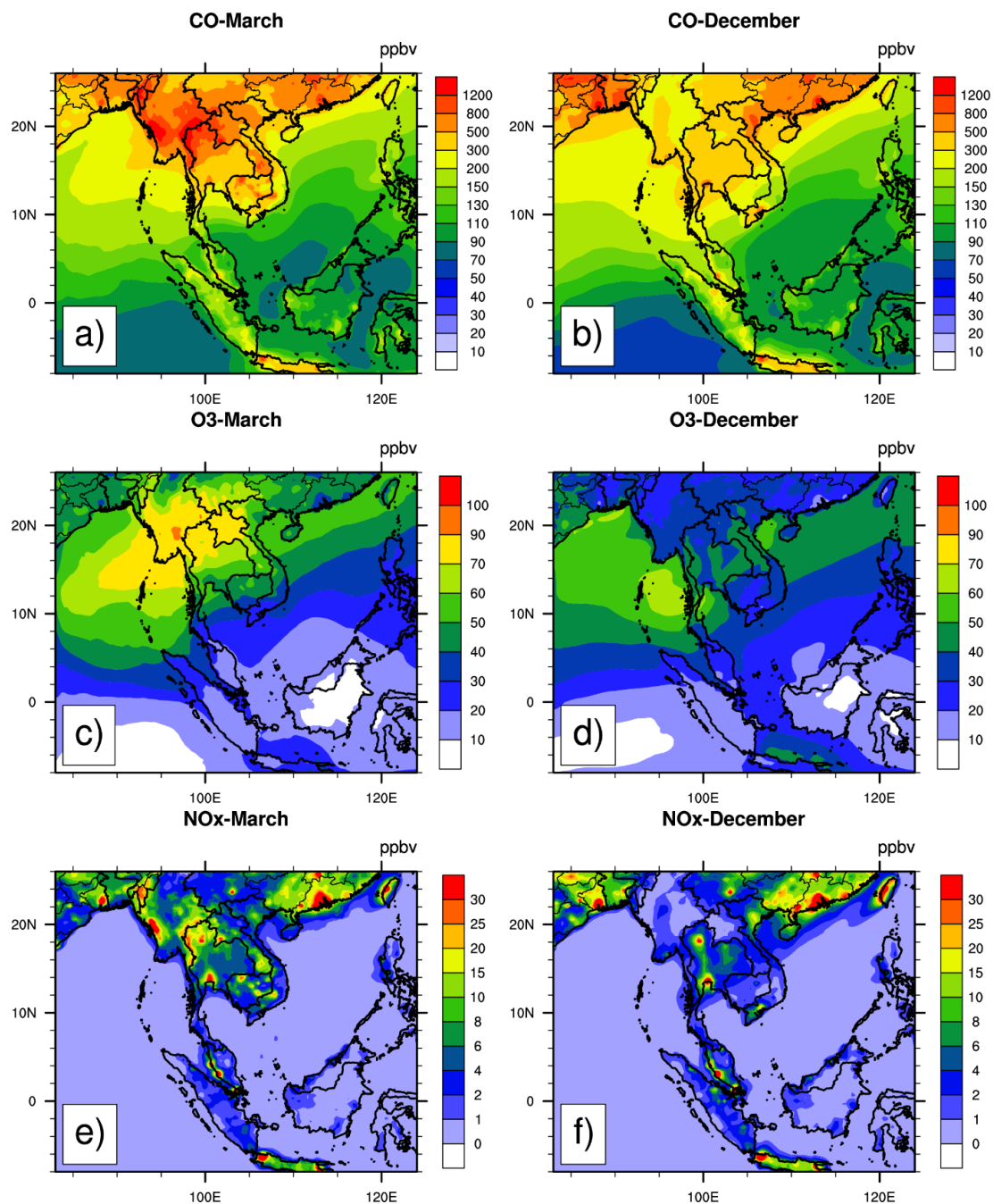
4



5

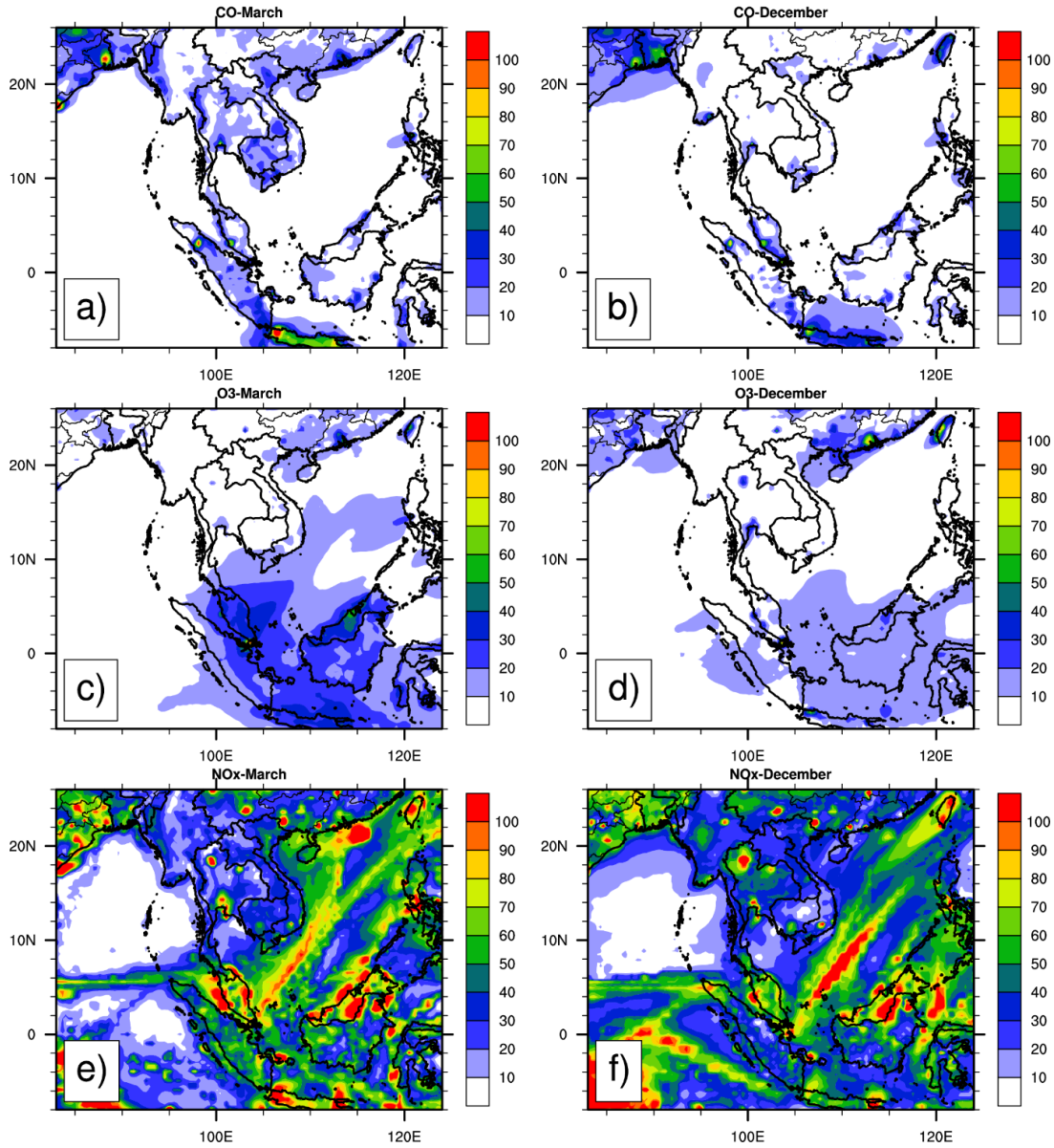
6 Figure 6. Accumulated precipitation (mm) a) GPCC, March, b) TRMM, March and c) WRF,  
7 March d) GPCC, December e) TRMM, December f) WRF, December.





1  
 2 Figure 7 Monthly-mean, surface mixing ratios for a) and b) CO, c) and d) O<sub>3</sub> e) and f) NO<sub>x</sub>  
 3 predicted by WRF-Chem using the averaged from 5 emission inventories for March (left) and  
 4 December (right panels) 2008.

## Variations (%)

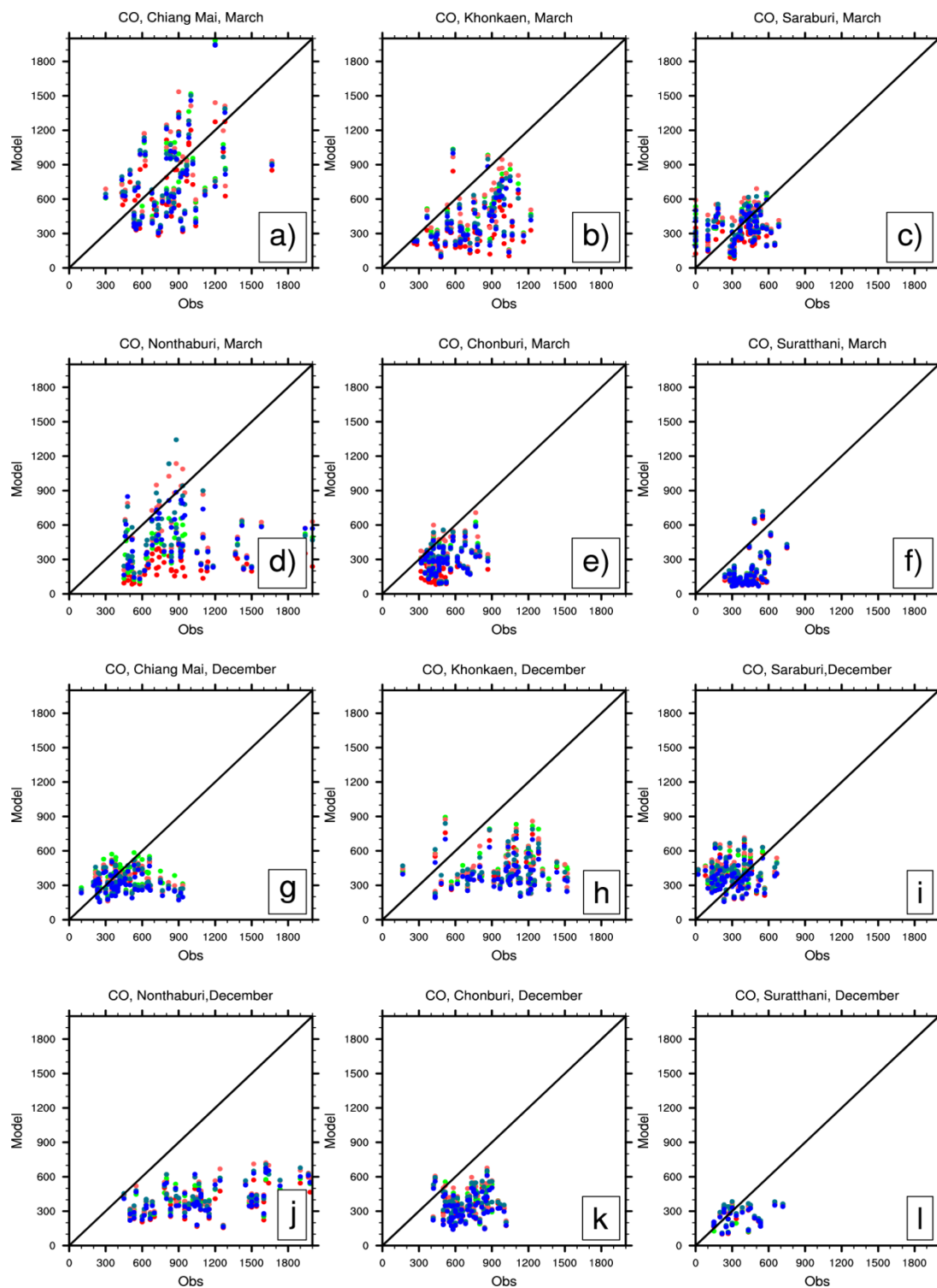


1

2 Figure 8 Variations, surface mixing ratios for a) and b) CO, c) and d) O<sub>3</sub> e) and f) NO<sub>x</sub>  
3 predicted by WRF-Chem using the averaged from 5 emission inventories for March (left) and  
4 December (right panels) 2008.

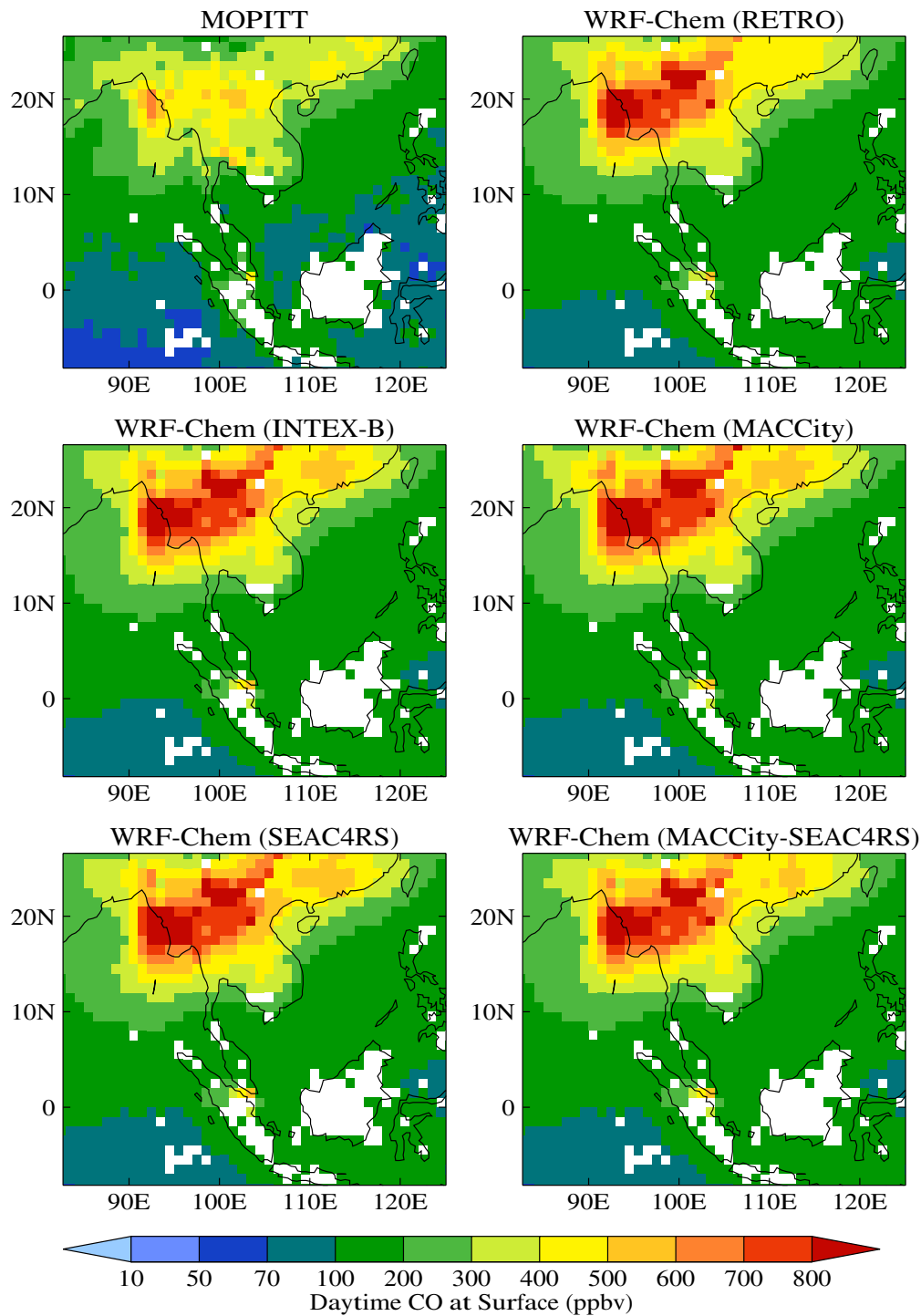
5

6



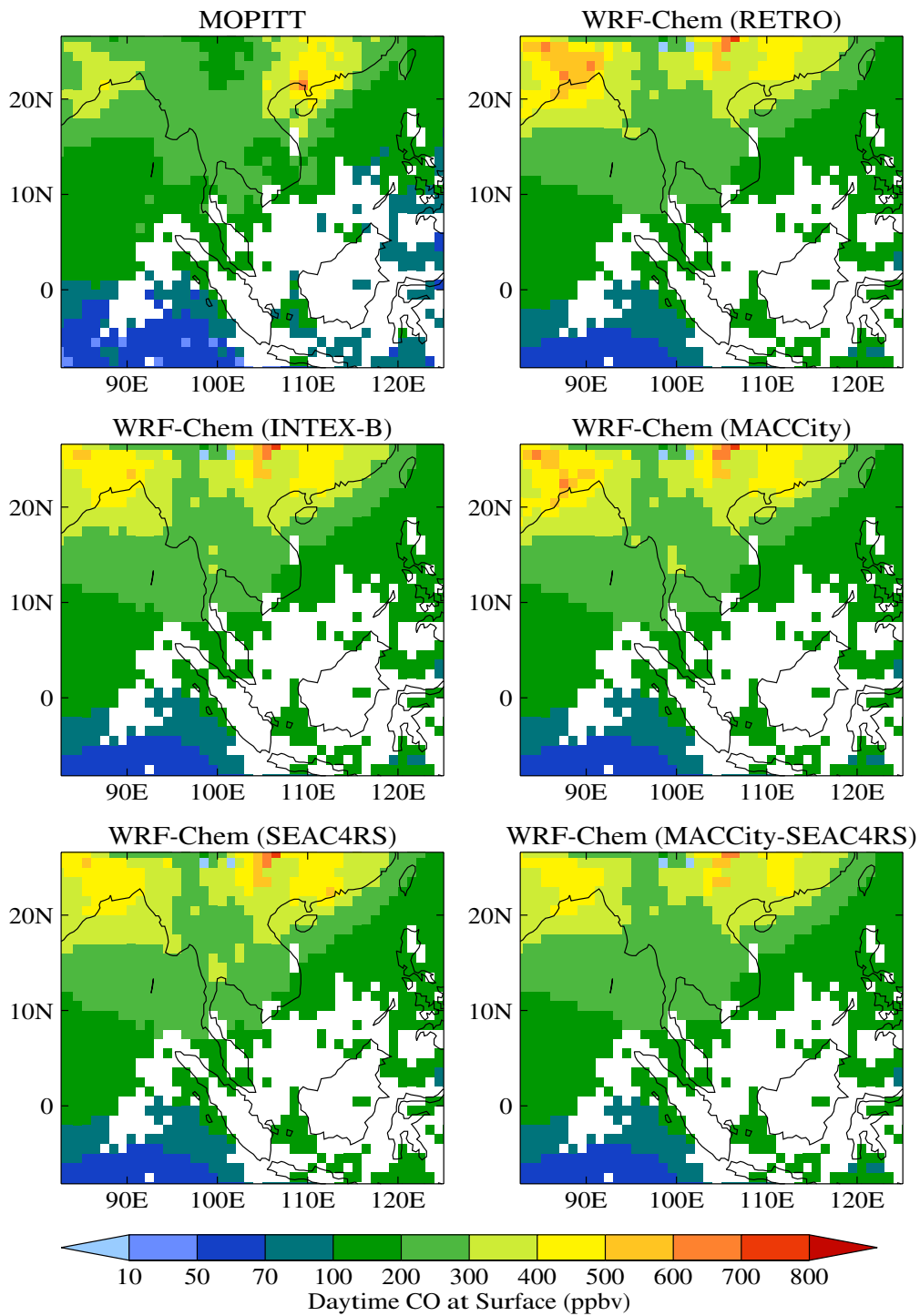
1  
 2 Figure 9. Scatter plots of 6-hourly daytime CO from WRF-Chem using different emissions  
 3 inventories (red dots are RETRO emissions, teal dots are SEAC4RS, orange dots MACCcity,  
 4 green dots INTEX-B, and blue dots are combined MACCcity and SEAC4RS) and ground-  
 5 based observations for March and December.

6

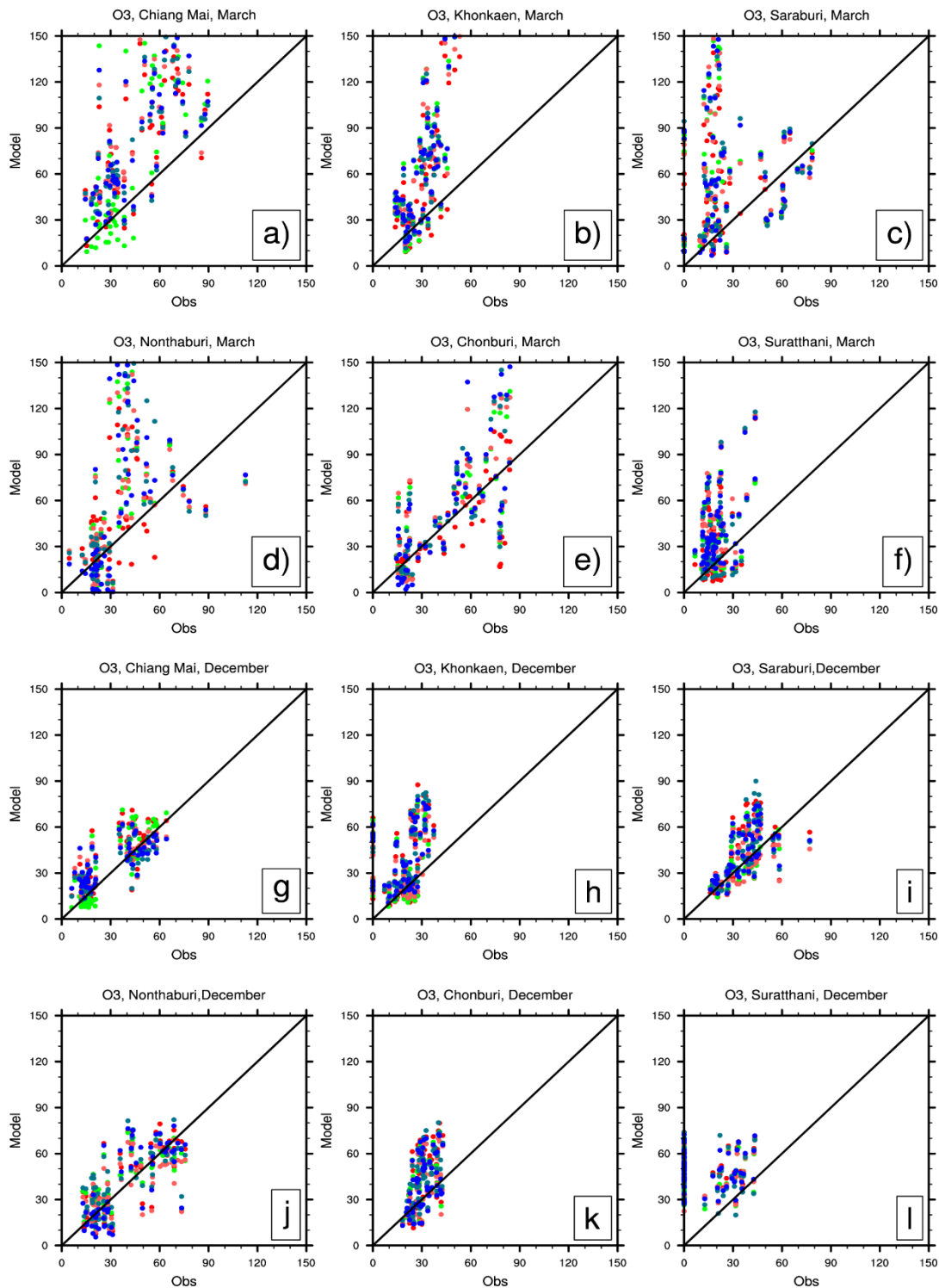


1  
 2 Figure 10 Carbon Monoxide from WRF-Chem and MOPITT in March a) MOPITT b) WRF-  
 3 Chem Simulation with RETRO emission inventory, c) WRF-Chem Simulation with INTEX-  
 4 B emission inventory, d) WRF-Chem Simulation with MACCCity emission inventory, e)  
 5 WRF-Chem Simulation with SEAC4RS emission inventory, e) WRF-Chem Simulation with  
 6 MACCCity/SEAC4RS emission inventory.

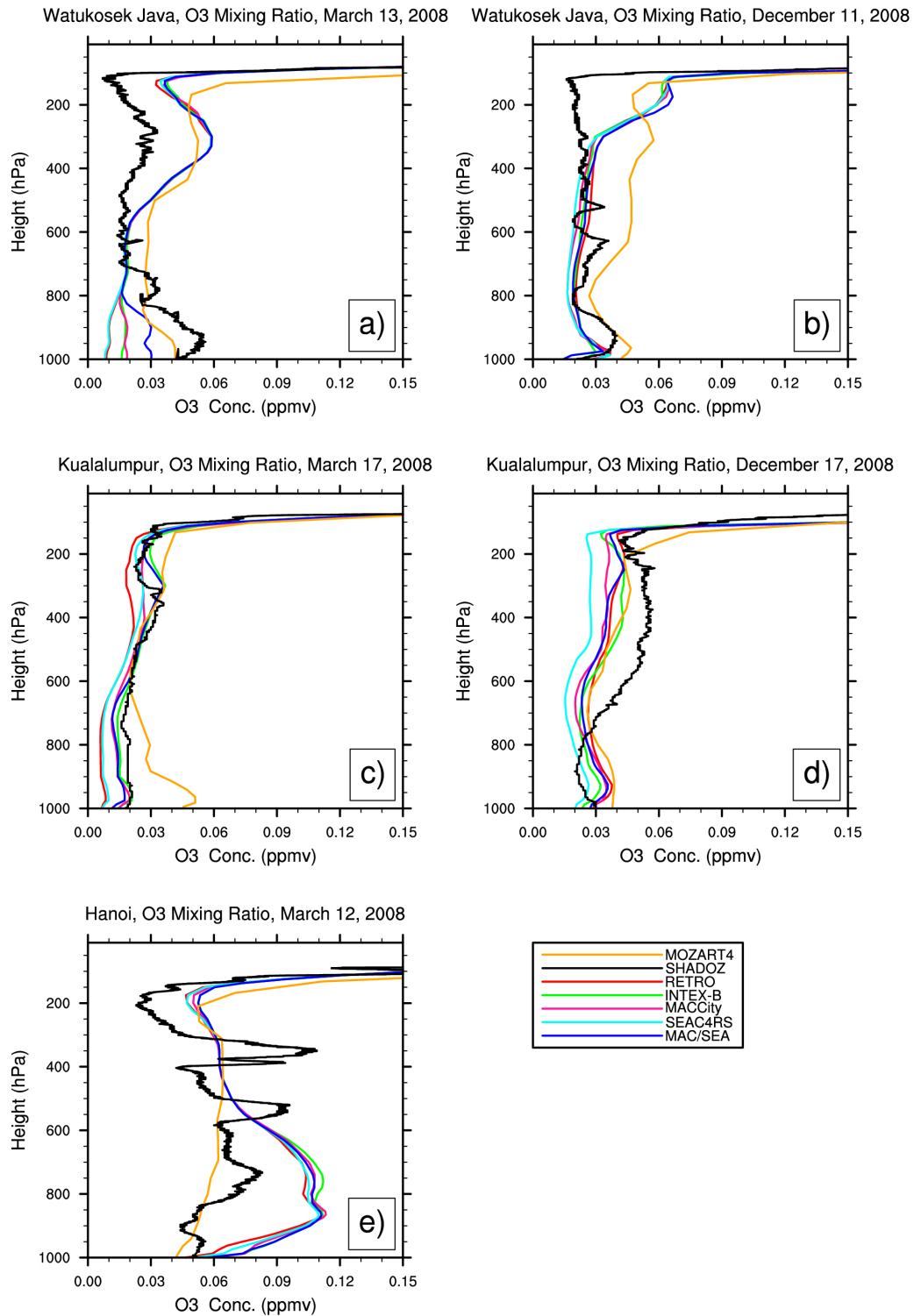
7



1  
2 Figure 11 Same as Fig.10 but for December.



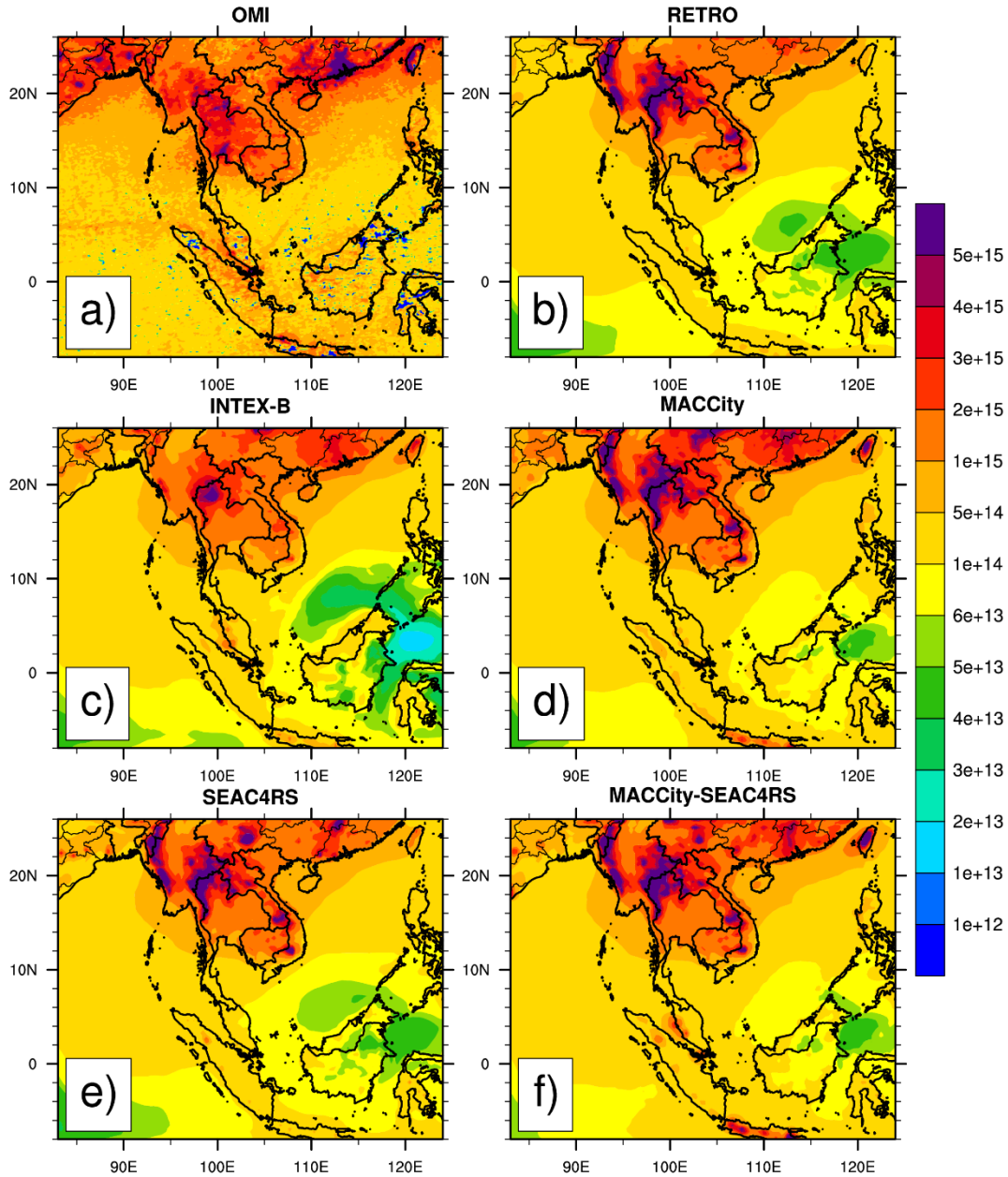
1  
 2 Figure 12. Scatter plots of 6-hourly daytime O<sub>3</sub> from WRF-Chem using different emissions  
 3 inventories (red dots are RETRO emissions, teal dots are SEAC4RS, orange dots MACCcity,  
 4 green dots INTEX-B, and blue dots are combined MACCcity and SEAC4RS) and ground-  
 5 based observations for March and December.



1

2 Figure 13. O<sub>3</sub> vertical profiles from WRF-Chem, MOZART4, and ozonesondes at three  
 3 SHADOZ ozonesonde locations for a) Watukosek-Java, Indonesia in March, b) Watukosek-  
 4 Java, Indonesia in December, c) Kuala Lumpur, Malaysia in March, d) Kuala Lumpur,  
 5 Malaysia in December, and e) Hanoi, Vietnam in March. Note that there are no SHADOZ  
 6 data at Hanoi during December 2008.

# Monthly NO<sub>2</sub> Total Column (molecule/cm<sup>2</sup>), March

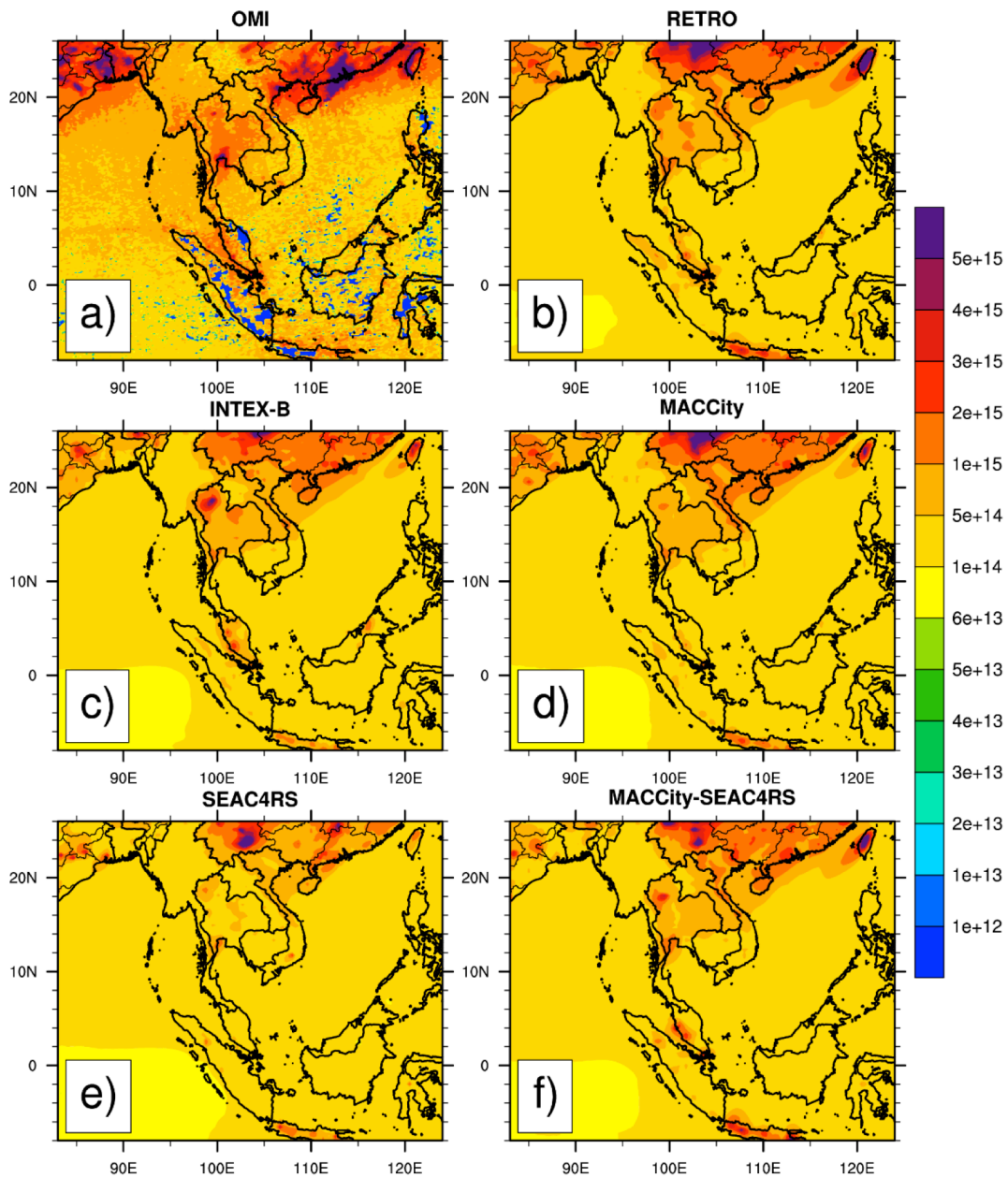


1

2 Figure 14 March 2008 monthly NO<sub>2</sub> total column a) OMI b) WRF-Chem + RETRO c) WRF-  
3 Chem + INTEX-B d) WRF-Chem + MACCity e) WRF-Chem + SEAC4RS f) WRF-Chem +  
4 MACCity-SEAC4RS.



# Monthly NO<sub>2</sub> Total Column (molecule/cm<sup>2</sup>), December



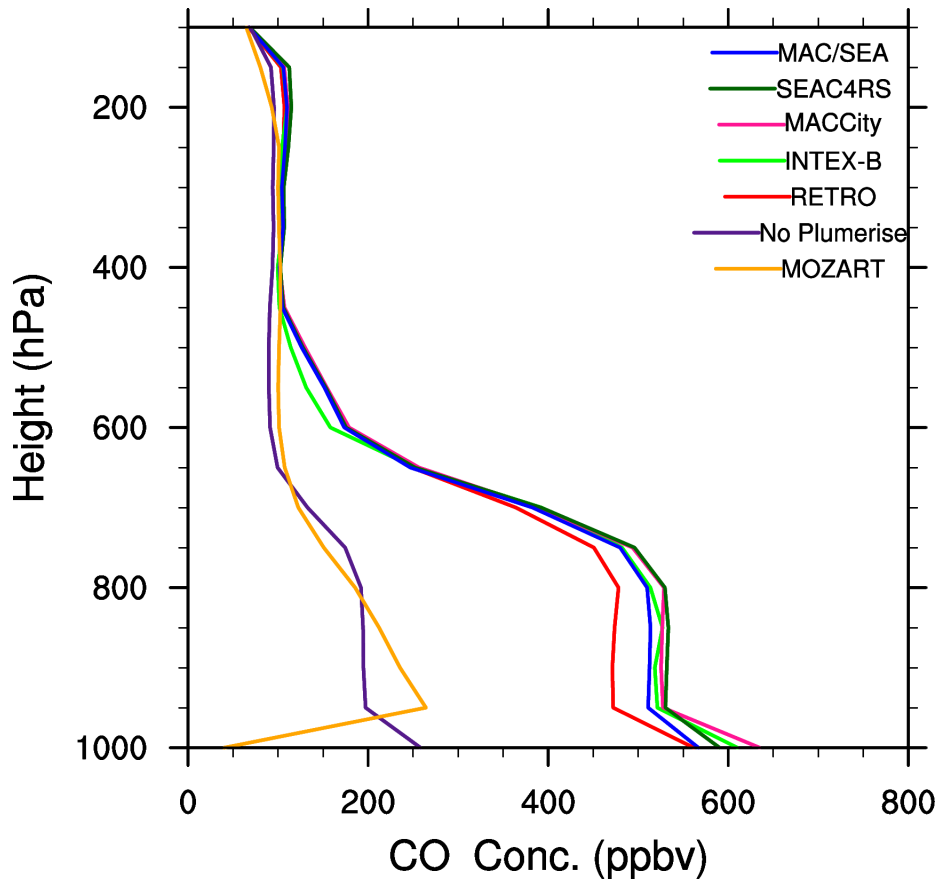
1

2

3 Figure 15 Same as Figure 19 but for December.

4

## Yangon, CO Mixing Ratio, March



1

2 Figure 16. March monthly-averaged CO vertical profiles at Yangon, Burma. WRF-Chem  
3 results with the plumerise feature of biomass burning emissions are given for the  
4 MACCity/SEAC4RS emissions case (blue line), SEAC4RS emissions (dark green line),  
5 MACCity emissions (red line), INTEX-B emissions (green line), and RETRO emissions (dark  
6 red line). The MOZART global model results are shown as the gold line. WRF-Chem results  
7 without the plumerise feature (i.e. biomass burning emissions injected into the lowest model  
8 level) are shown as the purple line.

9

1 Table 1 Emission sectors used in the model simulations from each emission inventory.

RETRO	INTEX-B	MACCity	SEAC4RS
1. Power Generation	1. Power plant	1. Energy production and distribution	1. Residential
2. Residential	2. Industry	2. Industry(combustion and non-combustion)	2. Industry
3. Industrial combustion	3. Residential	3. Land transport	3. Power
4. Industrial processes	4. Transportation	4. Maritime transport	4. Transport
5. Extraction of fossil fuels		5. Aviation	
6. Solvent use		6. Residential and commercial	
7. Road transport		7. Solvents	
8. Other mobile sources		8. Agriculture	
9. Waste treatment and disposal		9. Agricultural waster burning on fields	
10. Agriculture and Landuse change		10. Waste	

2

3

1 Table 2. Summation of CO emissions and NO emissions (mole km<sup>-2</sup> hr<sup>-1</sup>) from all grids in the  
 2 model domain for each month.

Emission Inventory	E_CO (mole km <sup>-2</sup> hr <sup>-1</sup> )		E_NO (mole km <sup>-2</sup> hr <sup>-1</sup> )	
	March	December	March	December
RETRO – 2000	410,840	496,860	30,590	39,320
INTEX-B – 2006	396,170	406,240	27,410	29,640
MACCity – 2010	436,750	454,250	27,440	28,280
MACCity/SEAC4RS	319,420	320,310	29,810	30,910
SEAC4RS – 2012	305,542	300,369	16,610	17,290
Biomass Burning – 2008	717,940	58,780	10,220	700
RETRO-Ship	3,404	3,364	5,097	5,186
INTEX-B-Ship	5,888	5,785	3,273	3,301
MACCity-Ship	3,569	3,717	3,980	5,138
REAS v1 <sup>a</sup> – 2000	282,120		13,828	

3 <sup>a</sup>REAS v1 emissions are from the ECCAD web site (<http://eccad.sedoo.fr>) and are the annual  
 4 emissions converted to hourly emissions assuming constant emissions for the year over the  
 5 WRF-Chem model domain.

6

7

1 Table 3. Monthly-average correlation coefficients (r) of daytime (00, 06, 12 UTC) CO.

Emission Inventories	CM		KK		SRB		NTB		CBR		SRT	
	Mar	Dec	Mar	Dec	Mar	Dec	Mar	Dec	Mar	Dec	Mar	Dec
RETRO	0.49	0.13	0.35	0.10	0.27	0.15	0.40	0.31	0.48	0.15	0.52	0.03
INTEX-B	0.51	0.14	0.42	0.20	0.17	0.17	0.33	0.38	0.44	0.17	0.58	0.03
MACCity	0.50	0.14	0.45	0.10	0.11	0.19	0.26	0.33	0.43	0.19	0.55	0.003
SEAC4RS	0.48	0.15	0.42	0.04	0.09	0.18	0.21	0.33	0.42	0.18	0.52	0.01
MACCity/ SEAC4RS	0.48	0.15	0.41	0.07	0.12	0.14	0.26	0.33	0.44	0.14	0.54	0.004

2

3

4 Table 4. Monthly-average biases of daytime (00, 06, 12 UTC) CO.

Emission Inventories	CM		KK		SRB		NTB		CBR		SRT	
	Mar	Dec	Mar	Dec	Mar	Dec	Mar	Dec	Mar	Dec	Mar	Dec
RETRO	-104	-147	-396	-581	-219	-314	-721	-770	-253	23	-267	-89
INTEX-B	-16	-114	-316	-529	-150	-283	-662	-747	-203	46	-234	-109
MACCity	-18	-112	-292	-530	-116	-263	-636	-733	-195	60	-238	-112
SEAC4RS	-22	-107	-324	-548	-129	-267	-645	-734	-197	58	-234	-120
MACCity/ SEAC4RS	-47	-157	-35	-601	-165	-328	-674	-785	-218	10	-243	-93

5

6

7

8

1 Table 5. Monthly-average correlation coefficients of daytime (00, 06, 12 UTC) O<sub>3</sub>.

Emission Inventories	CM		KK		SRB		NTB		CBR		SRT	
	Mar	Dec	Mar	Dec	Mar	Dec	Mar	Dec	Mar	Dec	Mar	Dec
RETRO	0.69	0.84	0.68	0.34	0.56	0.50	0.47	0.71	0.11	0.52	0.49	0.16
INTEX-B	0.74	0.89	0.72	0.33	0.70	0.48	0.45	0.72	0.05	0.56	0.44	0.09
MACCity	0.68	0.78	0.71	0.33	0.69	0.48	0.44	0.68	0.02	0.55	0.43	0.08
SEAC4RS	0.70	0.79	0.73	0.42	0.75	0.56	0.41	0.71	0.001	0.49	0.45	0.14
MACCity/ SEAC4RS	0.70	0.78	0.73	0.37	0.76	0.52	0.48	0.78	0.02	0.54	0.45	0.08

2

3

4

5 Table 6. Monthly-average biases of daytime (00, 06, 12 UTC) O<sub>3</sub>.

Emission Inventories	CM		KK		SRB		NTB		CBR		SRT	
	Mar	Dec	Mar	Dec	Mar	Dec	Mar	Dec	Mar	Dec	Mar	Dec
RETRO	36.48	8.28	23.83	19.36	7.77	13.58	12.15	3.07	17.82	6.96	9.52	31.29
INTEX-B	37.76	4.05	32.62	18.26	15.31	12.42	18.54	2.67	23.64	5.58	14.57	29.56
MACCity	39.67	6.19	30.24	15.68	14.62	8.69	18.53	-1.34	24.88	3.04	15.76	30.36
SEAC4RS	38.53	3.75	31.45	20.14	17.29	13.98	27.90	4.61	24.38	6.33	11.26	29.15
MACCity/ SEAC4RS	39.72	5.31	32.45	19.92	16.59	13.37	18.19	-0.25	24.95	5.52	15.38	32.22

6

7

8

1 Table 7. Monthly-average surface O<sub>3</sub> and CO mixing ratios at land-based grid points in  
 2 Southeast Asia.

Emission Inventories	CO (ppb)		O <sub>3</sub> (ppb)	
	March	December	March	December
RETRO	571	596	146	122
INTEX-B	575	497	156	119
MACCity	574	495	160	122
SEAC4RS	574	494	159	122
MACCity/SEAC4RS	575	495	154	115

3